A Universal Model for Halftone Reflectance

Patrick Noffke*, John Seymour*

Keywords: dot gain, TVI, halftone, color, CIELAB, Murray-Davies

Abstract

The Murray-Davies equation was originally invented to model the color of hard dots. It has long served as a process control device to monitor dot gain on a web offset press. More recently, it has migrated to alternate forms of printing where the dots are no longer crisp, with well-defined edges. The calculation received a new name when this happened: TVI. Unfortunately, the equation itself was not updated to reflect the wide range of dot sharpness. The equation was never all that accurate at predicting the actual color of a halftone. Furthermore, as dots soften and blend together to form more of a continuous tone, the prediction gets worse.

The limitations of TVI and the Murray-Davies formula are described in this paper. Two alternate mathematical models are considered: one based on the assumption that a dot thins as it spreads, and the other the Yule-Nielsen equation. These two models yield results that are suprisingly similar. The fact that both equations are very close to linear in CIELAB leads to a third mathematical model which is strictly empirical, but computationally simpler.

This model is used to characterize print from numerous types of presses. In most cases, the prediction error is less than 1 ΔE^*_{ab}, as compared with prediction errors which are often greater than 5 ΔE^*_{ab} when the Murray-Davies equation is used.

Murray-Davies (Hard Dot Model)

Dot gain is an important process control parameter, giving the press operator a way to objectively determine whether a press is printing properly, or at least consistently. The original concept is simple. Halftone dots grow in size through the printing process. Dot gain is simply a measure of the change in size of the dot as the dot goes from film to plate to print. Theoretically at least, one can measure dot gain by use of a microscope and imaging system. Such a device, called a dot planimeter, was in use as early as 1961.

From a practical standpoint, a densitometer or spectrophotometer provides a much simpler means to indirectly measure the size of the dot. Density measurements are made of the halftone, of the paper, and of the solid. A simple calculation based on the Murray-Davies formula is used to determine the size of the theoretical dot that would give the measured density.

In Figure 1, let us say that the magenta dots cover 20% of the area on the plate. Let's say that the reflectance of the paper is 90%, and the reflectance of the solid magenta ink is 5%. There are two components to the reflectance of the halftone, the reflectance contribution of the paper and that of the dots.

The reflectance contribution of the dots is the area of the halftone times the reflectance of the solid, that is 20%x5%=1%. The reflectance contribution of the paper is the area of the paper (100%-20%=80%) times the reflectance of the paper, that is 80%x90%=72%. Thus, the Murray-Davies estimate of the reflectance of the halftone is 1%+72%=73%.

This simple computation is an illustration of the Murray-Davies equation, which is given by

$$R_{ht}(a,\lambda) = (1-a)R_p(\lambda) + aR_s(\lambda) \tag{1}$$

where $R_{ht}(a,\lambda)$ is the reflectance at wavelength λ of a halftone region with dots having area a, $R_p(\lambda)$ is the reflectance of the paper, and $R_s(\lambda)$ is the reflectance of a solid ink region on the same paper. From here on out, we will drop the parameters a and λ, and use R_{ht} in place of $R_{ht}(a,\lambda)$, and R_p and R_s for the reflectance of the paper and solid, respectively. This leads to the dot gain equation, which is used to measure the effective dot area a_{eff} of a given halftone.

$$a_{eff} = \frac{R_{ht} - R_p}{R_s - R_p} \tag{2}$$

*QuadTech, Sussex, WI, USA

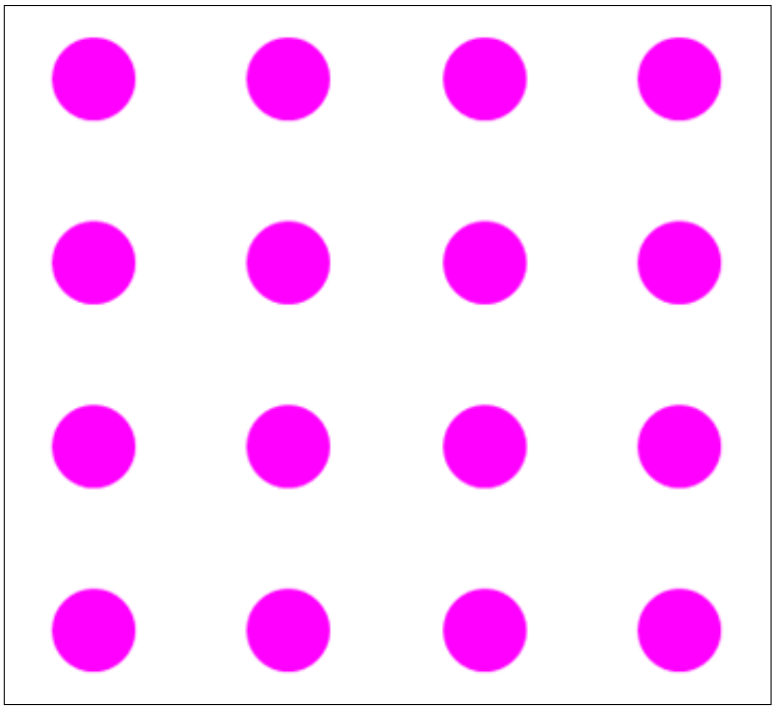

Figure 1: Illustration of a magenta halftone pattern

The dot gain, or TVI, is then given by

$$TVI = a_{eff} - a = \frac{R_{ht} - R_p}{R_s - R_p} - a \tag{3}$$

Limitations of Murray-Davies Equation

The Murray-Davies equation can be used to estimate reflectance for any effective dot area. Figure 2 demonstrates one of the limitations of the Murray-Davies equation. This figure shows the measured and estimated reflectance of a magenta 50% tone patch, along with two other curves labeled "Murray-Davies (no TVI)" and "Beer's Law" (more on the latter shortly). The data was obtained from an IT8.7/4 patch target printed with web offset, on a coated paper with matte finish. The estimated reflectance was calculated using the Murray-Davies equation with TVI values of 10%, 15%, and 20%. Notice how the *shape* of the measured reflectance is somewhere between that of the Murray-Davies (no TVI) and the Beer's Law curves. This is an important clue. Different values of TVI essentially shift the estimated curve up and down in the wavelengths below 600 nm, but do not achieve the shape of the measured curve. As can be seen from the ΔE^*_{ab} values shown on the graph, the Murray-Davies equation does not do a particularly good job at estimating the spectrum of a magenta halftone.

Figure 3 demonstrates another limitation. (Data courtesy of Dr. Guenter Bestmann, Heidelberger Druckmaschinen.) This figure shows the measured reflectance vs. wavelength for a 50% cyan halftone, along with the estimated reflectance of a 53% and a 66% halftone, calculated using the Murray-Davies equation. This graph shows that if one were to use the standard formula (based on the Murray-Davies equation) to compute TVI within the red wavelength range of 600 to 650 nm, this particular sample would have a TVI of 16%. If one were to use the blue wavelength range of 450 to 500 nm, then the TVI would be 3%. One would not expect the size of a halftone dot to be dependent on wavelength.

While the Murray-Davies TVI is not necessarily meaningful in the physical sense, it is still possible to make it a number that is useful for process control. To do this, it is necessary to define the wavelength range where one is to make the computation. The Status T or E density filters have historically been used, which incorporate the wavelength ranges where each ink has its strongest absorption (e.g. 590 to 650 nm for cyan). With the advent of profiles, and particularly of profiles that have been smoothed or otherwise adjusted, the density values are often not available. If TVI is to be determined from XYZ values, it is necessary to go to special lengths to determine numbers which agree with Status T or E. Methods for this conversion are described in (ISO 10128, Appendix A) and in (Seymour, 2008).

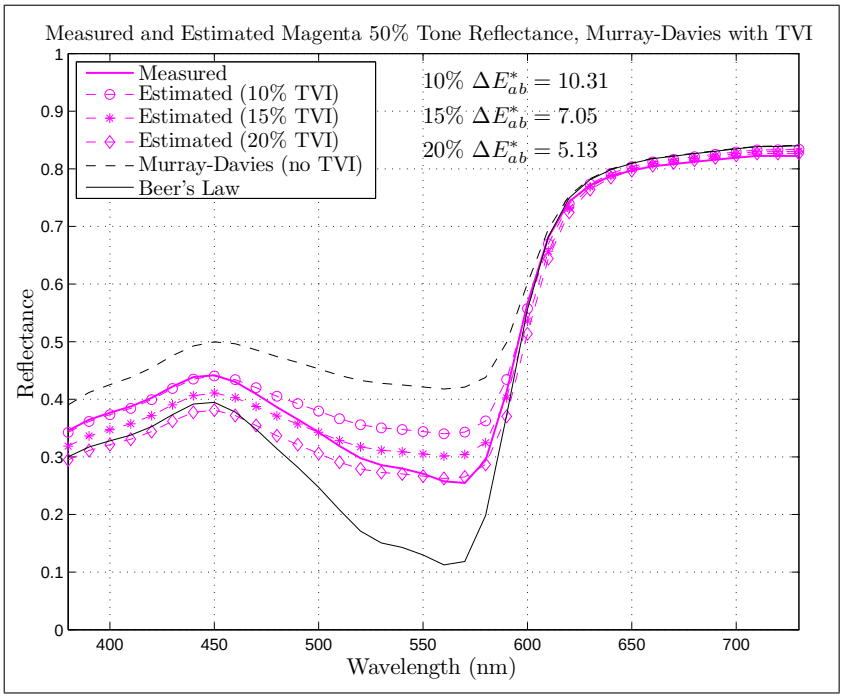

Figure 2: Magenta 50% tone reflectance, estimating reflectance using the Murray-Davies equation with 10%, 15%, and 20% TVI. The shape of the measured reflectance does not match Murray-Davies or Beer's Law.

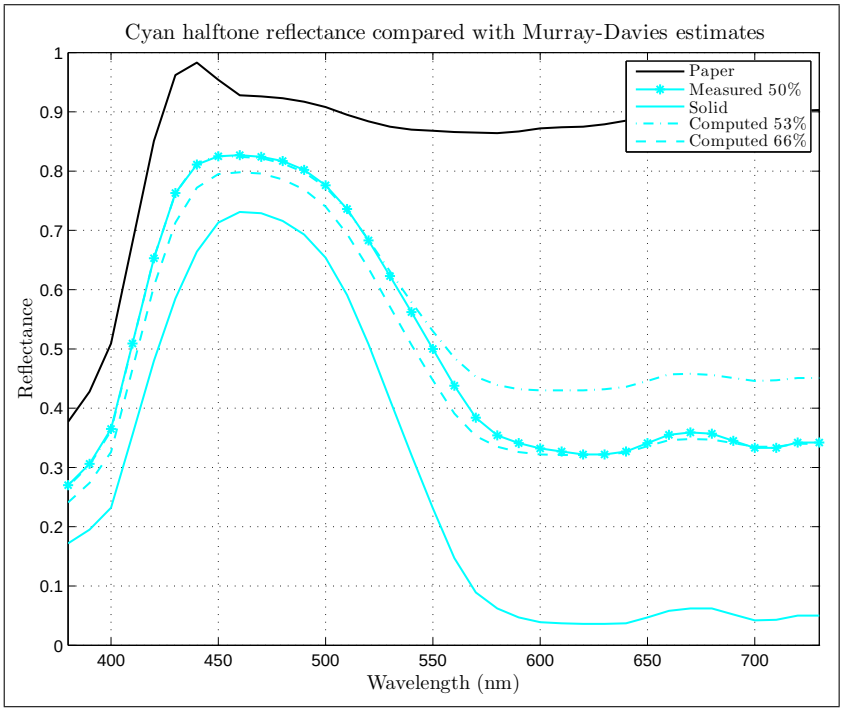

Figure 3: Comparison of measured spectrum of a cyan halftone with two spectra estimated with Murray-Davies. In the red wavelengths, the TVI is 16%, and in the blue wavelengths, the TVI is 3%.

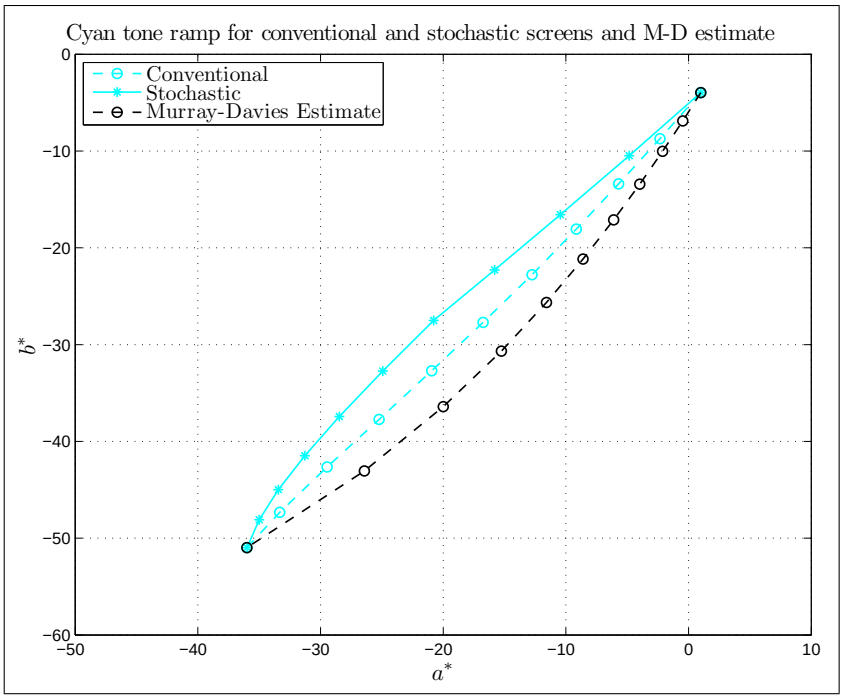

Figure 4: Comparison of conventional and stochastic screening tone ramp with Murray-Davies estimate. With TVI, the estimated (a^*, b^*) value moves along the black Murray-Davies curve.

Figure 4 shows an (a^*, b^*) plot of a Murray-Davies estimate of a tone ramp for cyan, along with measurements of actual tone ramps for conventional screening and stochastic screening. The dots are all spaced at 10% increments of tone value. (Data courtesy of Dr. Bestman.) Figure 4 demonstrates an important point. If TVI is used to improve the estimate, the (a^*, b^*) value will move along the curve shown for the Murray-Davies estimate. The Murray-Davies equation (with TVI) is only accurate to within 3 to 4 ΔE^*_{ab} for conventional halftoning and barely to within 5 ΔE^*_{ab} for stochastic. No matter what TVI is used to predict the color of a cyan 50%, the equation will not do a good job of predicting the color of a 50% halftone.

It is common practice to use plate curves to correct one print process so as to produce the same color as another. Figure 4 suggests the limitation of this. In particular, a plate curve cannot be expected to make stochastic printing look like conventional. The discrepancy in the tone ramps between conventional and stochastic led Dr. Bestman to conclude that these two screening types require different profiles (Bestman, 2011).

Beer's Law (Continuous Tone Model)

Beer's Law may be used to provide a different estimate of the reflectance of a halftone. The assumption here is that there is a given volume of ink (as dictated by the original dot size), and that this ink spreads out evenly to a continuous tone. This ink is thinner than the ink layer for the solid, but covers more area. Beer's Law is used to give an estimation of the relationship between the resulting ink film thickness and the reflectance of the halftone area, as was illustrated in Figure 2.

It is recognized that Beer's Law is a simplification of the physics involved with light reflecting from a printed area. Beer's Law assumes that light passes into the ink layer where it is selectively absorbed, reflects from the paper, is selectively absorbed as it passes through the ink layer again, and then is emitted from the ink. The equation describes the probability that a photon is absorbed as a function of the ink film thickness.

Beer's Law does not account for the fact that light also reflects directly from the surface of the ink, and it does not account for the fact that light may scatter within the ink and be emitted without ever reaching the paper. While these two effects are generally small, they can be significant for inks that are either very dark or very thick.

More sophisticated equations have been developed to describe the relationship between ink film thickness and reflectance. The

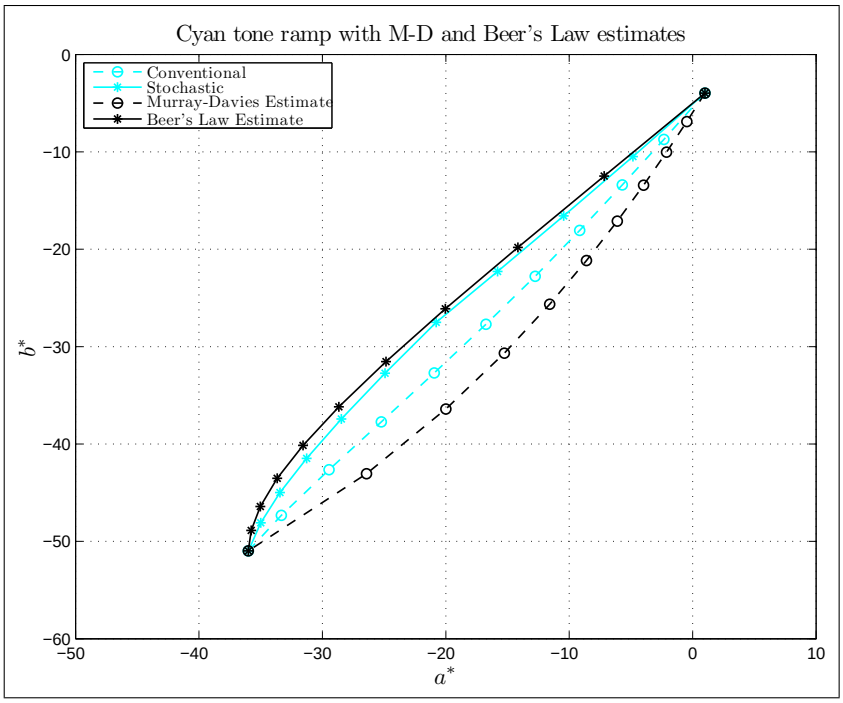

Figure 5: Comparison of conventional and stochastic tone ramps with two estimates, Murray-Davies and Beer's Law. The shape of the Beer's Law estimate closely matches that of the stochastic data.

Kubelka-Munk equations are a theoretical set of equations that have been used (for example) to predict the color of a mixture of pigments. The empirical Tolenaar-Ernst equation has also shown good success in predicting density as a function of ink film thickness. Still, the Beer's Law approximation has proven to be a useful approximation in certain circumstances (Seymour, 2007).

Here is the Beer's Law equation

$$R_{ht} = \left(\frac{R_s}{R_p}\right)^a R_p \tag{4}$$

Figure 5 is a reprise of Figure 4, with the addition of the Beer's Law estimate of the tone ramp. Figure 6 is based on the same data, only presenting it from a different perspective. The x-axis of the graph is the paper-relative chroma, and the y-axis is the L^* value.

It is clear from Figures 5 and 6 that (at least for this data set) Beer's Law provides a good approximation to the shape of the tone ramp curve for stochastic printing. Conventional printing lies roughly midway between the Murray-Davies estimate and the Beer's Law estimate.

Hypothesis

One is tempted to hypothesize that all single-ink halftone printing falls conveniently between these two mathematical models. This is worth investigating. Several data sets from different printing processes were investigated. Note that since the Beer's Law estimate is best computed from spectral data (see Appendix A and (Viggiano, 2010)), it was not possible to use the wealth of profile data sets available.

Web Offset, Conventional and Stochastic Screening

The data represented in Figures 4, 5, and 6 have been "delicately massaged" to smooth the data, and to adjust the paper and solids to predetermined aim points. As such, there is a chance that the massaging introduced some subtle artifact. Figures (7, 8, and 9)

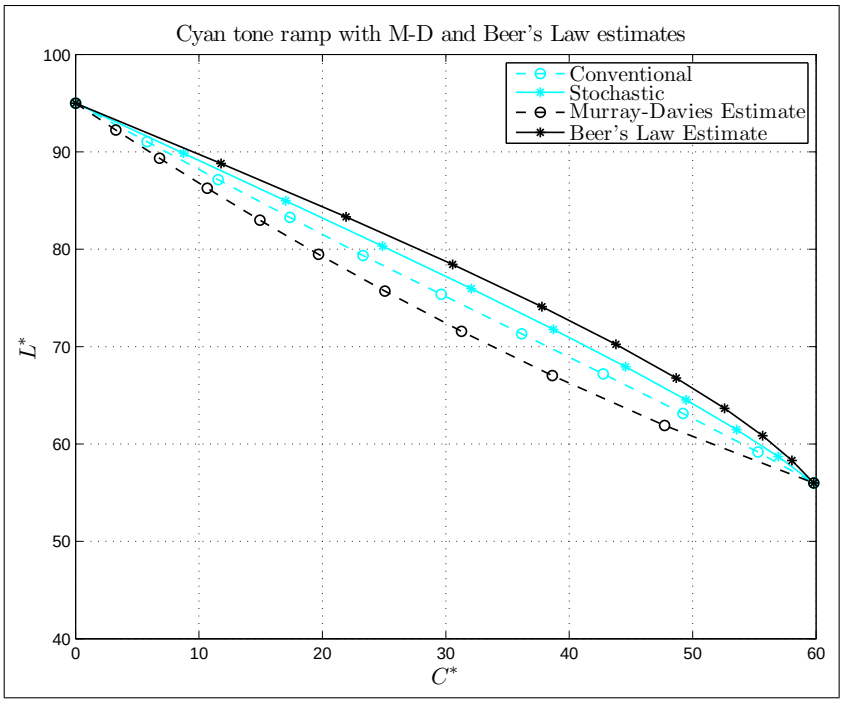

Figure 6: Same data as Figure 5, but plotting L^* as a function of chroma.

were derived from data provided by Mike Rodriguez (formerly of RR Donnelley) that had not been adjusted. These graphs all appear very similar to the data from Dr. Bestman, and they all support the hypothesis.

Figures (10, 11, and 12) were derived from data from the IT8.7/4 patch target that was used for Figure 2. These graphs also support the hypothesis.

Gravure

Bob Hallam of Quad Graphics provided spectral data of tone ramps that were printed on a gravure press. The (a^*,b^*) plots of these data are shown in Figures 13, 14, and 15. The overall appearance of these graphs is very similar to all those seen so far, with two exceptions. The first is that the gravure plots hug very closely to the Beer's Law estimation – even closer than the plots for stochastic printing. The second observation is that there are several data points in these graphs where the (a^*,b^*) values step just outside the region confined by the Murray-Davies and Beer's Law estimates. The reasons for this are unknown, but it is assumed that a more accurate substitute for Beer's Law may solve the discrepancy. Alternately, mottling may have distorted the measurement of the solids, or the discrepancy may just be the result of anomalous data.

Flexography

Tone ramps printed on a flexo press were provided by Corrugated Synergies International, of Reston, WA. These tone ramps were printed at three different screen rulings: 85 lpi, 110 lpi, and 126 lpi. Figures 16, 17, and 18 show the (a^*,b^*) plots for this data. We see that in terms of the *bananagrams*, this flexo run behaved very similar to conventional screening produced on a web offset press. This is not particularly surprising, considering that the dots have the same appearance as web offset dots when viewed through a loupe.

Conclusion on the Hypothesis

Thus far, the graphs suggest that the initial hypothesis is largely true. The printing of halftone ramps is contained between the Murray-Davies estimate and the Beer's Law estimate. Data from 25%, 50%, and 75% patches on coldset newsprint were analyzed and found to be approximated well by the Beer's Law estimate, but are not presented in this paper. Data from digital print has

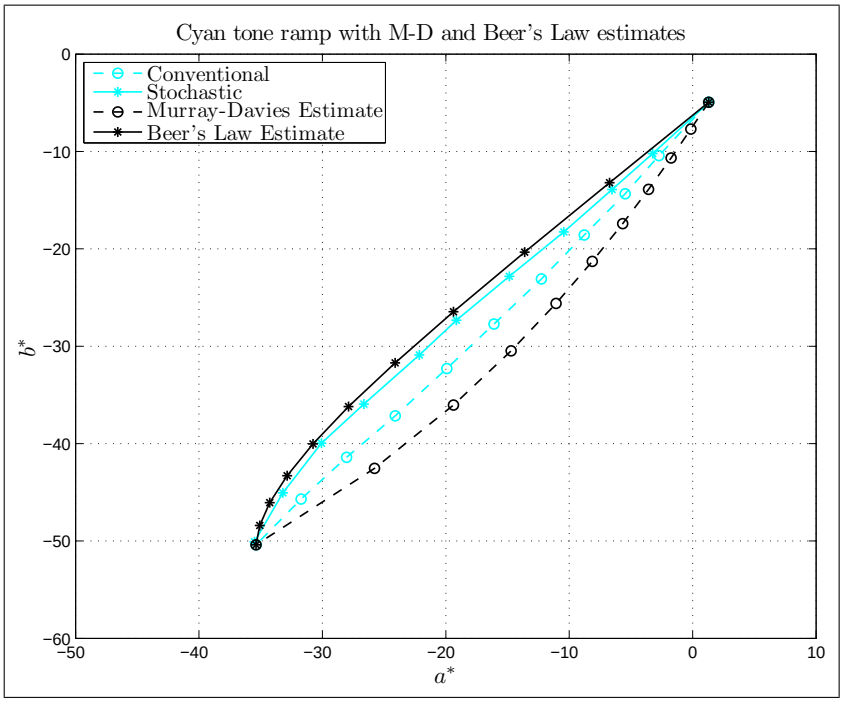

Figure 7: Cyan tone ramp, web offset, conventional and stochastic screens and Murray-Davies and Beer's Law estimates, data from Mike Rodriguez.

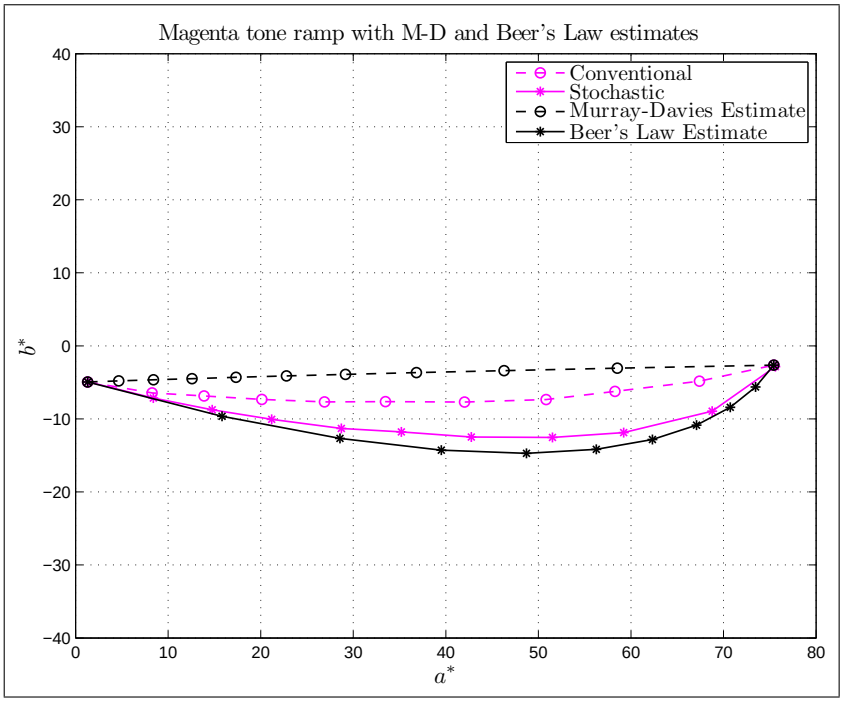

Figure 8: Magenta tone ramp, web offset, conventional and stochastic screens and Murray-Davies and Beer's Law estimates, data from Mike Rodriguez.

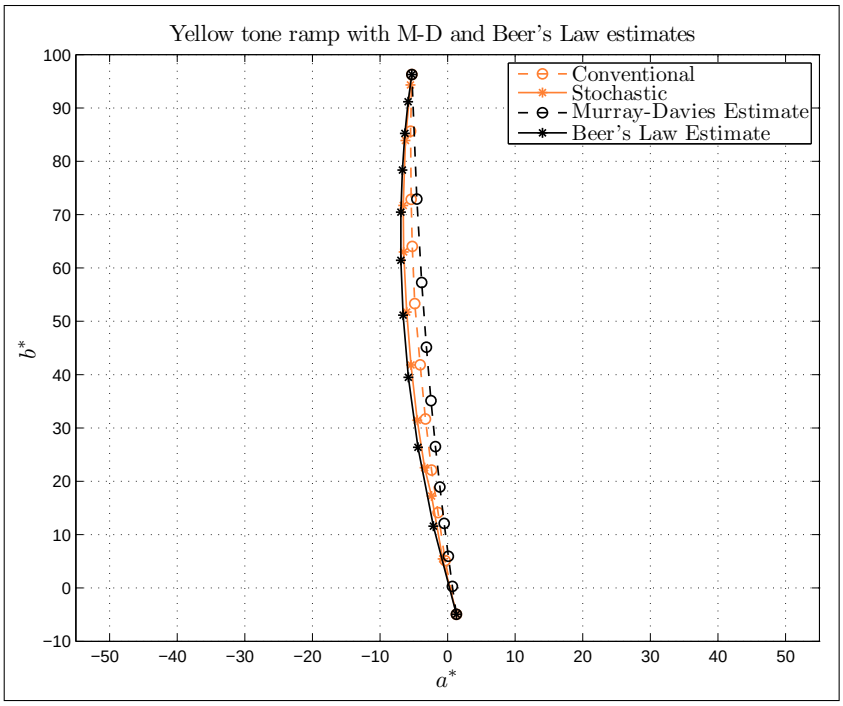

Figure 9: Yellow tone ramp, web offset, conventional and stochastic screens and Murray-Davies and Beer's Law estimates, data from Mike Rodriguez.

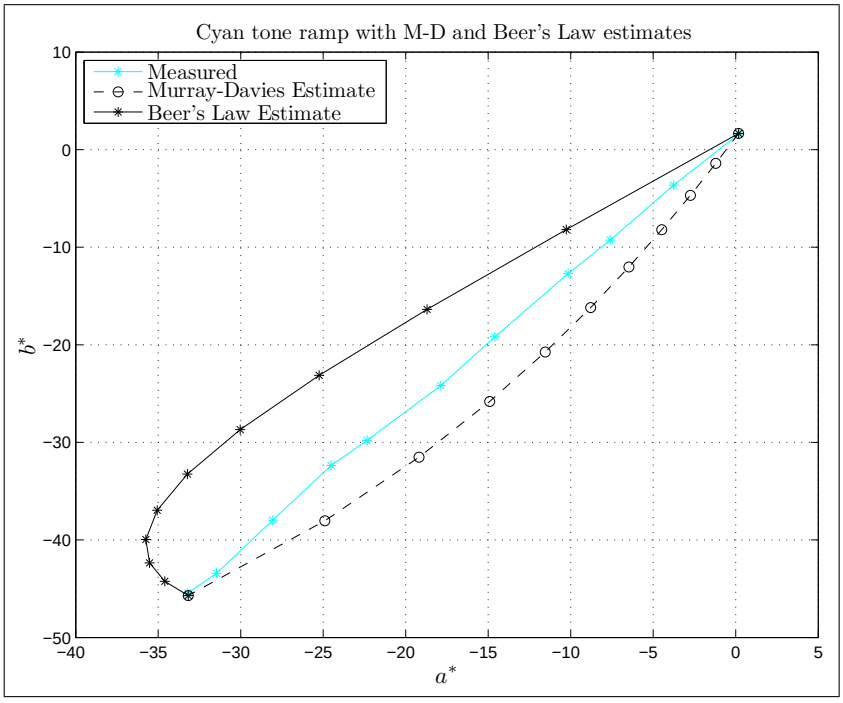

Figure 10: Cyan tone ramp, web offset, conventional screen and Murray-Davies and Beer's Law estimates, coated matte paper.

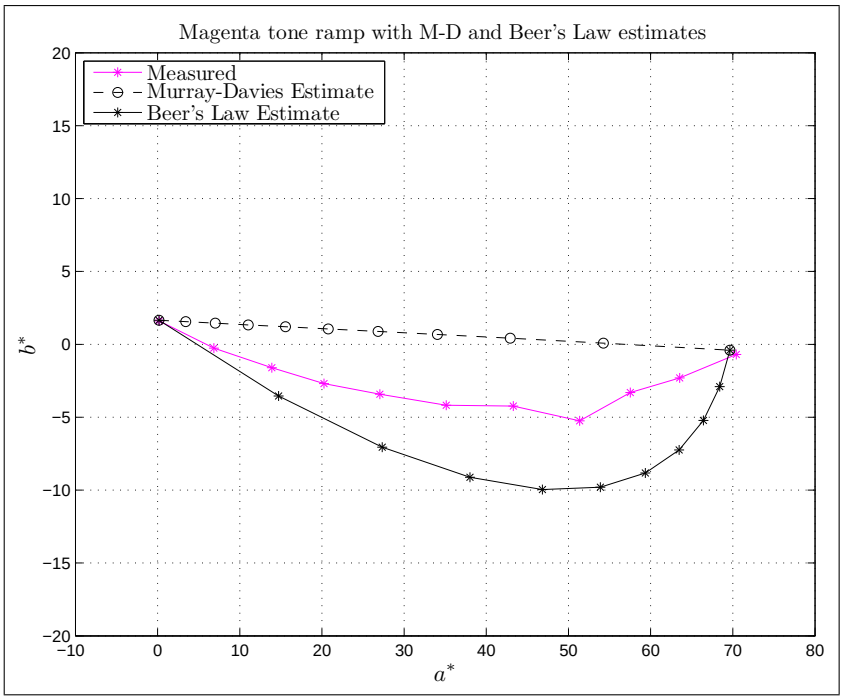

Figure 11: Magenta tone ramp, web offset, conventional and stochastic screens and Murray-Davies and Beer's Law estimates, coated matte paper.

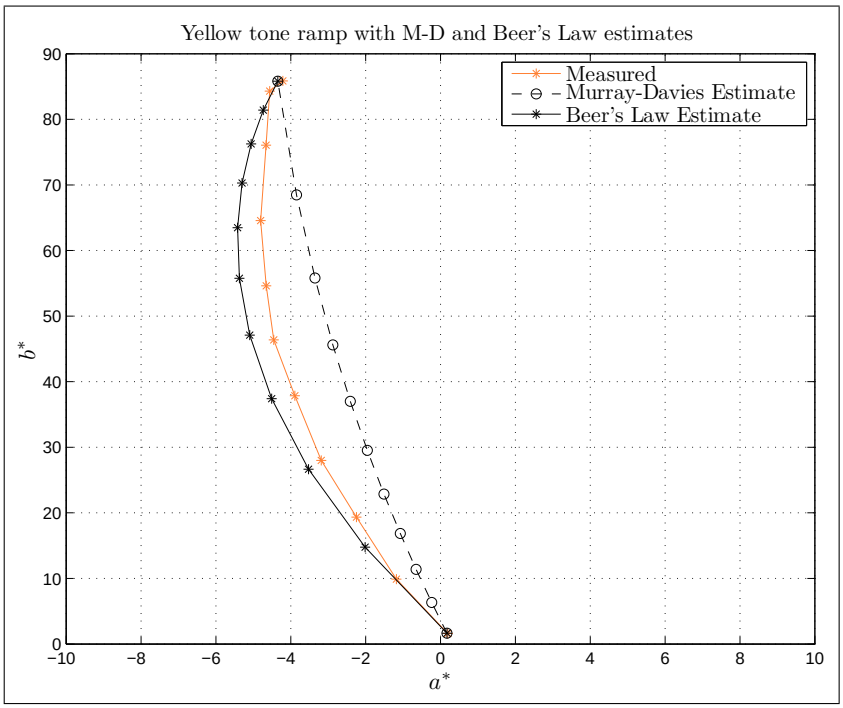

Figure 12: Yellow tone ramp, web offset, conventional and stochastic screens and Murray-Davies and Beer's Law estimates, coated matte paper.

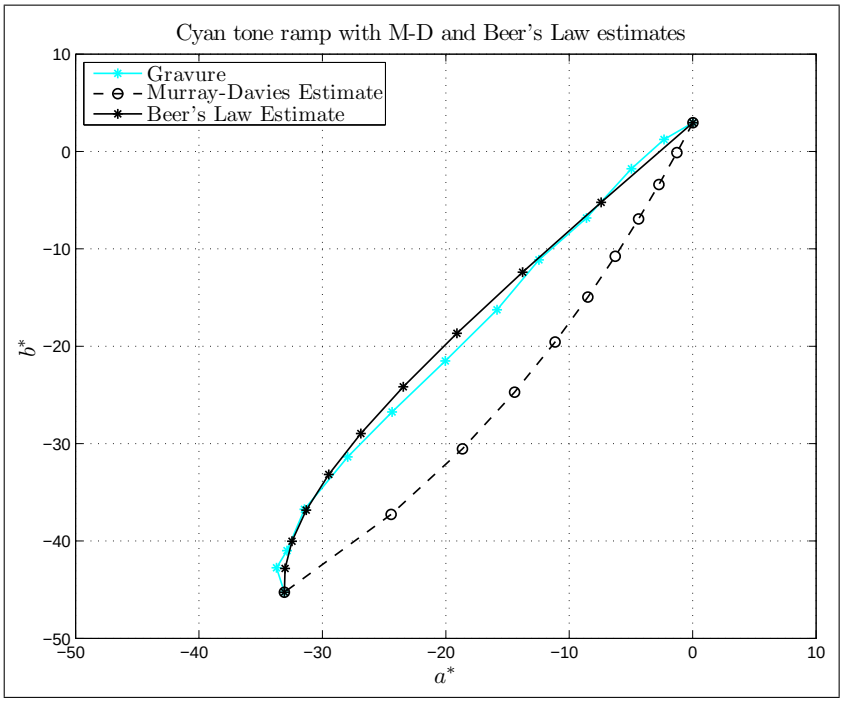

Figure 13: Cyan tone ramp, gravure data and Murray-Davies and Beer's Law estimates, data from Bob Hallam.

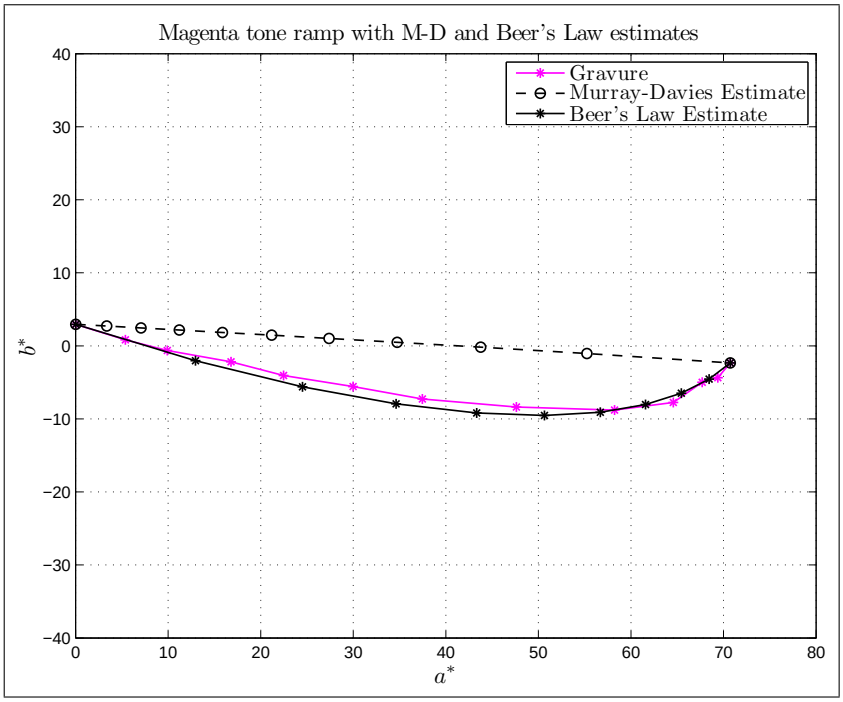

Figure 14: Magenta tone ramp, gravure data and Murray-Davies and Beer's Law estimates, data from Bob Hallam.

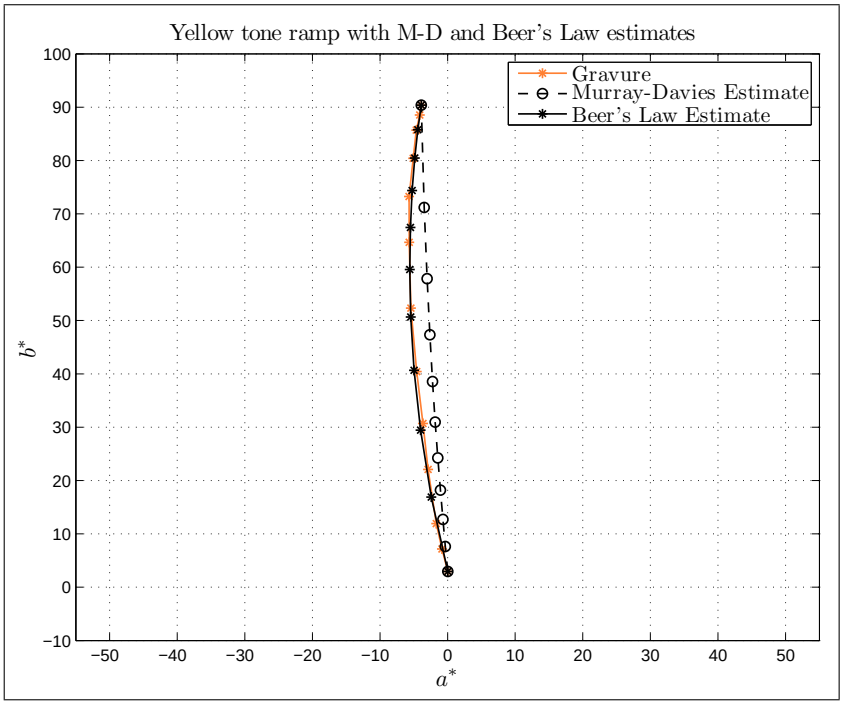

Figure 15: Yellow tone ramp, gravure data and Murray-Davies and Beer's Law estimates, data from Bob Hallam.

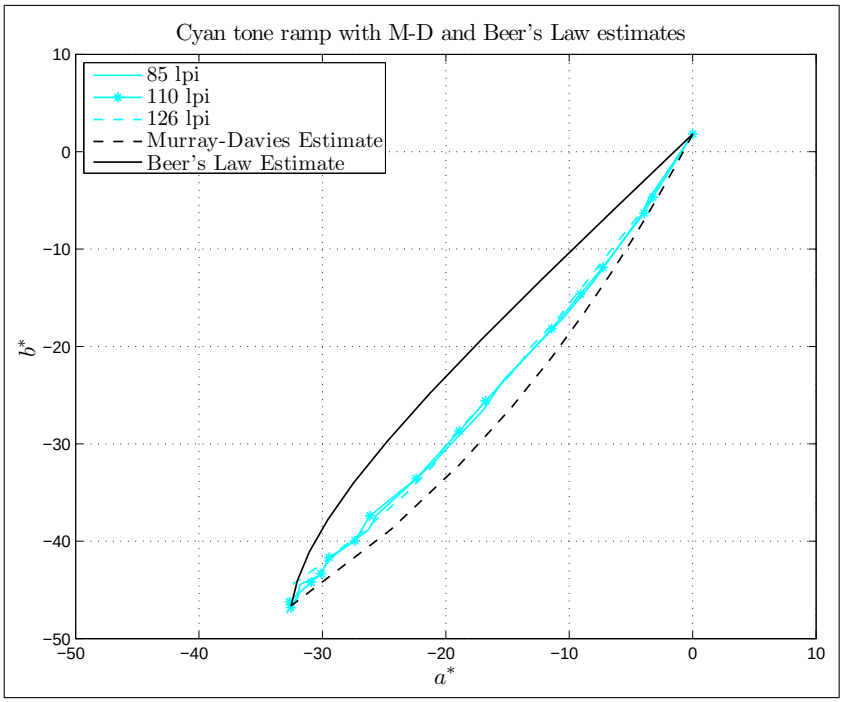

Figure 16: Cyan tone ramp, flexo data and Murray-Davies and Beer's Law estimates.

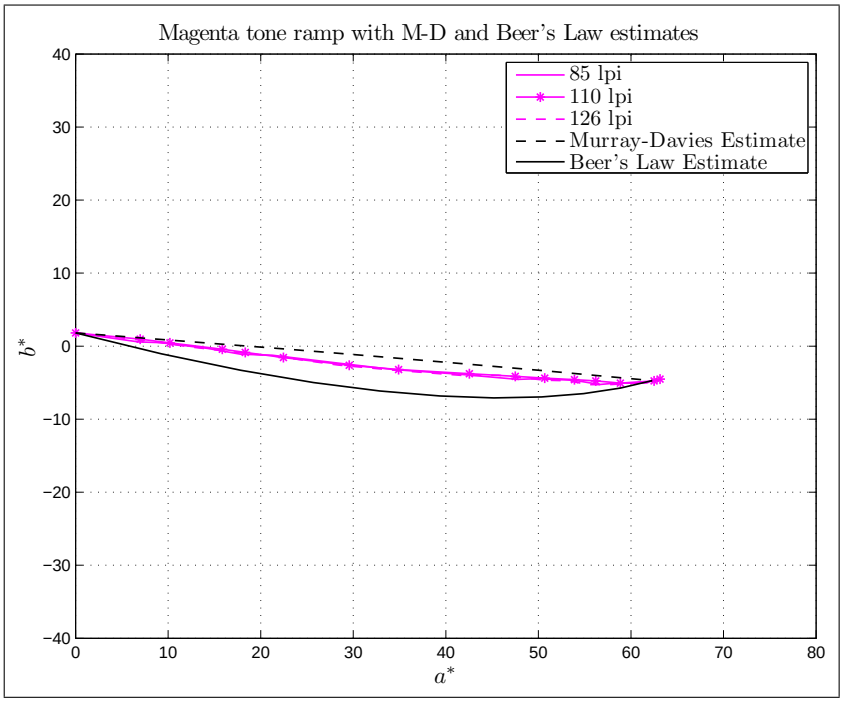

Figure 17: Magenta tone ramp, flexo data and Murray-Davies and Beer's Law estimates.

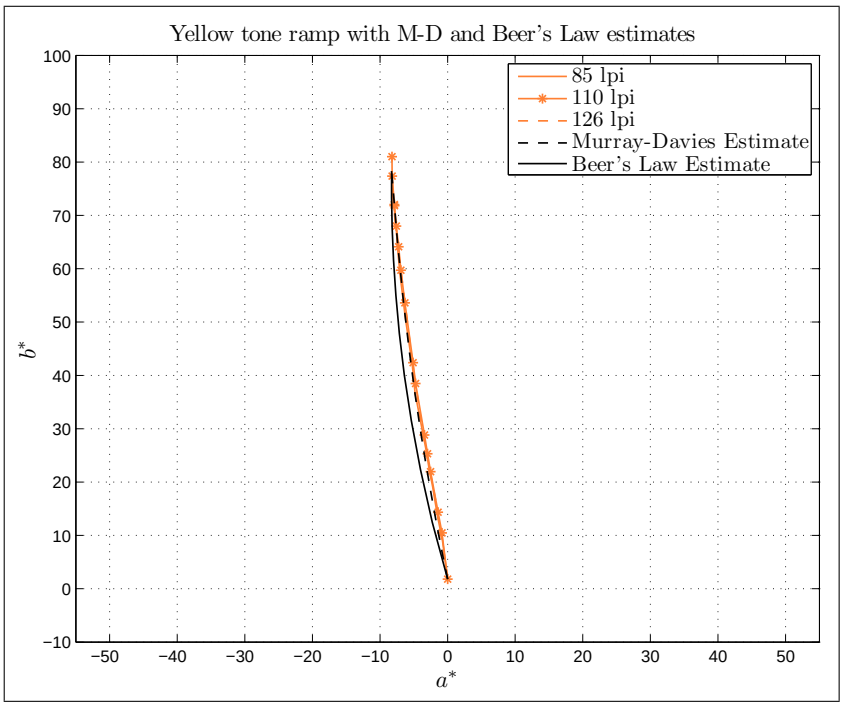

Figure 18: Yellow tone ramp, flexo data and Murray-Davies and Beer's Law estimates.

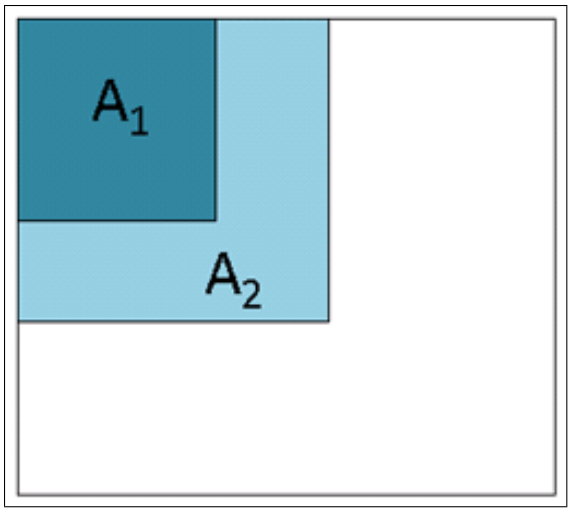

Figure 19: A dot on the plate, spread out to a larger area on the paper.

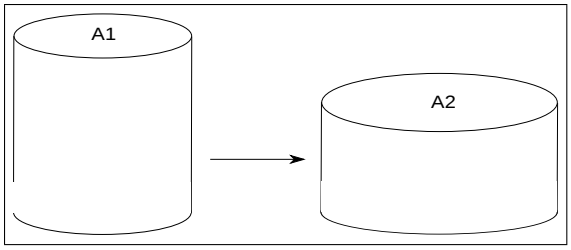

Figure 20: A dot of area $A1$ spreads out to have area $A2$ on the paper, maintaining constant volume.

not yet been analyzed.

Dot Spread Equation (Soft Dot Model)

We have been conditioned to think about dot gain (and TVI) strictly in terms of dots getting larger. We generally do not consider that for most print processes, there is a fixed amount of ink for any particular tone value. If the dot increases in size, it must decrease in ink film thickness. This concept of dot spread may be used to formulate another equation to model the reflectance of a halftone.

One such equation can be derived by making two simple assumptions:

1. Assume that the plate gets a uniform thickness of ink in the inked areas. That is, on the plate itself, the thickness of the ink on a halftone dot is equal to the thickness of the solid.
2. Assume further that the dot spreads out by the time it is transferred to the paper. By the law of conservation of ink volume, it will become both larger in area and smaller in thickness.

In this model, we will completely ignore the Yule-Nielsen effect, that says that the paper between dots takes on a slight tint of the dots because of light scattering in the paper.

Figures 19 and 20 illustrate the assumptions.

Suppose the area of the dot on the plate is a_1, with nominal thickness of 1.0 unit. The dot then spreads by some amount so that the area of the dot on the printed page is a_2. By the law of conservation of ink volume, the thickness of the larger area is a_1/a_2.

Beer's Law can be used to approximate the reflectance of the dot portion with this reduced thickness:

$$R_{dot} = \left(\frac{R_s}{R_p}\right)^{\frac{a_1}{a_2}} R_p \tag{5}$$

Substituting this into the Murray-Davies equation, we have:

$$R_{ht} = (1 - a_2)R_p + a_2 R_{dot} \tag{6}$$

or

$$R_{ht} = (1 - a_2)R_p + \left(\frac{R_s}{R_p}\right)^{\frac{a_1}{a_2}} R_p \tag{7}$$

Note that if $a_1 = a_2$ (there is no spread) then Equation 5 becomes $R_{dot} = R_s$, and Equation 6 reduces to Equation 1, the Murray-Davies equation. Note also that if $a_2 = 1$ (there is total spread so that the area is evenly covered), then Equation 6 reduces to $R_{ht} = R_{dot}$, which is Equation 4, the Beer's Law equation. So, as a_2 goes from a_1 to 1.0, the equation for a halftone reflectance transitions from a model of hard dots to a model of continuous tone.

With the standard Murray-Davies model there is one free parameter, the TVI, which can be determined from the reflectance of a given halftone along with that of the paper and the solid. The TVI can later be used to estimate the color of a given tone value when printed.

The dot spread model also has one free parameter, the *increase* in dot area. We will refer to $g = a_2 - a_1$ as the dot area increase, or DAI[1], where $a_1 + g \leq 1$. Then $a_2 = a_1 + g$, and we can then rewrite Equation 7 as

$$R_{ht} = (1 - a_1 - g)R_p + \left(\frac{R_s}{R_p}\right)^{\left(\frac{a_1}{a_1+g}\right)} R_p \tag{8}$$

Given the reflectance of a given halftone along with that of the paper and a solid region, g can then be determined and later used to estimate the color of a given tone value when printed. Thus, one model is a direct substitute for the other. One difference is that the Murray-Davies equation can be readily solved for the effective dot area. Equation 8 cannot be solved for g in closed form, so the determination of g must be done iteratively. The solution is obtained by finding that value of g which minimizes the difference between the estimated reflectance (or color) and the measured reflectance (or color) of the halftone.

Experimental Results

Using the coated, matte data that was shown in Figure 2 and Figures 10-12, we compared the performance of the Murray-Davies (with TVI) model with that of the dot spread model.

For the Murray-Davies model, we determined a best-fit TVI curve which minimizes the error between the measured and estimated reflectance. Past experience tells us that the shape of traditional TVI curves has been approximately parabolic, with a maximum TVI at or near 50% tone value. We used the *gain*, *lean*, and *bulge* parametric curves (see Appendix B) that allow the curve to change in magnitude, lean toward 0 or 1, and change the rate of decline from the peak value. The best-fit TVI curves are shown in Figure 21. These TVI values were then used to compute estimated reflectance, substituting the increased area (plate area plus TVI) into Equation 1. These reflectance estimates were used to compute CIELAB values, and the results were compared against the measured CIELAB values. The ΔE^*_{ab} vs. tone value for the Murray-Davies with TVI estimates are shown in Figure 22. The worst-case error is around 8.7 ΔE^*_{ab} for magenta at 70% tone value. The error for cyan has a maximum around 5.3 ΔE^*_{ab} at 60% tone value. Yellow is not too bad, with a maximum error of 3.2 ΔE^*_{ab}.

For the dot spread model, we would like to consider a model for how the dot spreads versus dot area. Since TVI curves are approximately parabolic, it seems reasonable to start with such a curve for dot area increase. We may want to allow for more spread for the lower tone values, since the smaller dots are not touching each other and have more room to grow in area. We

[1]We use DAI instead of TVI, since the latter implies a tone region "looks like" (in the Murray-Davies sense) a tone region with a higher dot area of the same thickness as a solid region.

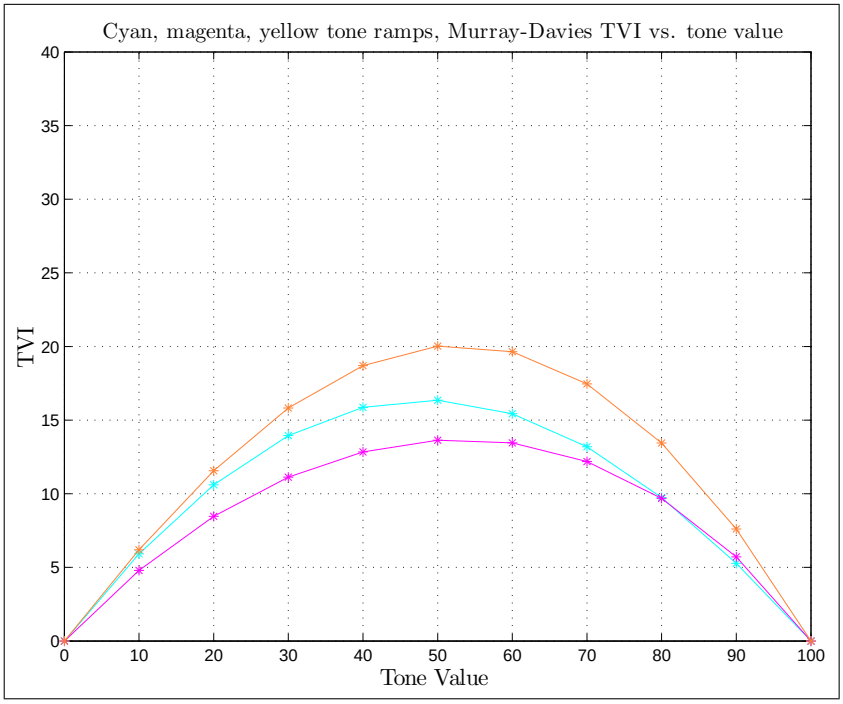

Figure 21: Cyan, magenta, yellow tone ramps, best-fit Murray-Davies TVI vs. tone value, coated matte data.

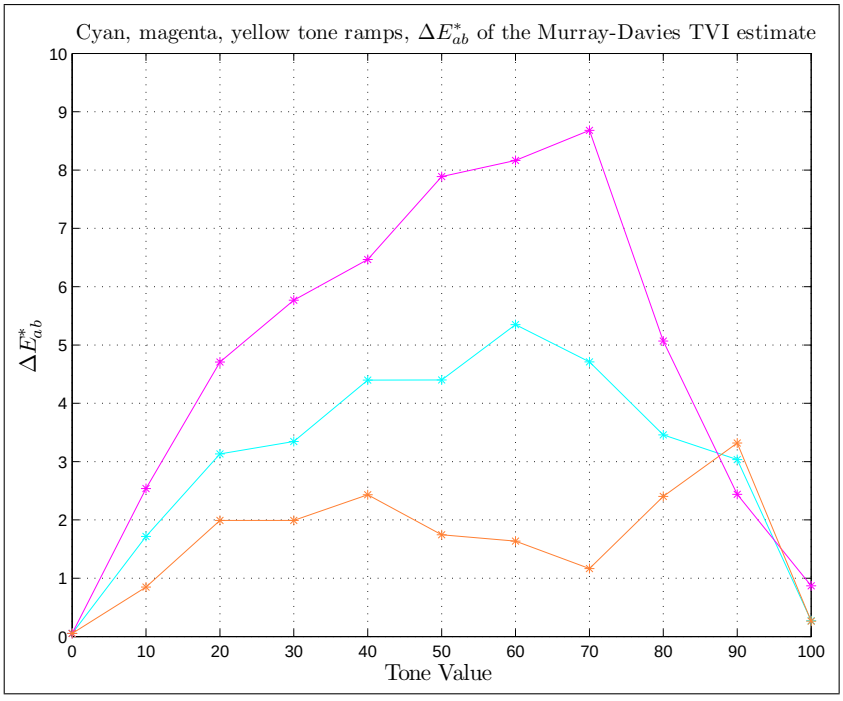

Figure 22: Cyan, magenta, yellow tone ramps, ΔE^*_{ab} values of the Murray-Davies TVI estimate, coated matte data.

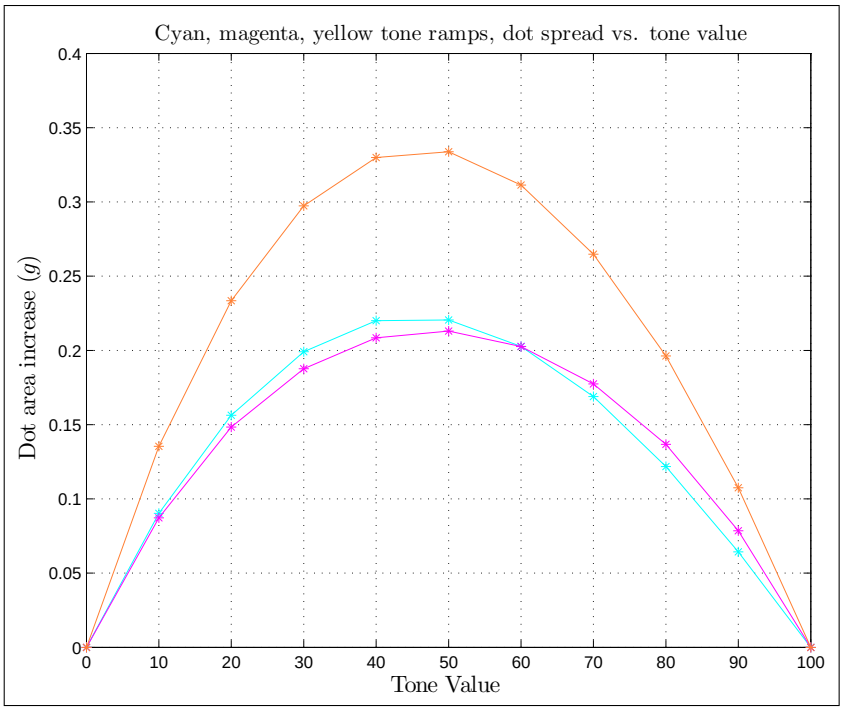

Figure 23: Cyan, magenta, yellow tone ramps, best-fit dot area increase vs. tone value, coated matte data.

	$gain_g$	$lean_g$	$bulge_g$
Cyan	22.1	1.7	-0.23
Magenta	21.3	0.58	0.67
Yellow	33.4	1.85	0.14

Table 1: Dot spread model, best-fit values of $gain_g$, $lean_g$, and $bulge_g$, for cyan, magenta, and yellow tone ramps, coated matte paper.

again use the parametric curves described in Appendix B. We will refer to these parameters as $gain_g$, $lean_g$, and $bulge_g$, with the g subscript denoting the dot area increase curve parameters.

Optimization was performed to determine the values for $gain_g$, $lean_g$, and $bulge_g$ that minimize the error between the measured and estimated reflectance, for each of the ink tone ramps. Table 1 shows the best-fit values for these parameters. The dot area increase curves vs. tone value are shown in Figure 23. The $lean_g$ values are all positive (the curves lean to the left), indicating a tendency for smaller dots to have more spread.

The estimated reflectance was then computed using the best-fit dot area increase curve, $g(a)$, and substituting the value for g into Equation 8 for each tone value. These reflectance estimates were used to compute CIELAB values. The (a^*, b^*) plots for cyan, magenta, and yellow are shown in Figures 24-26. These figures are essentially the same as Figures 10-12, with the addition of the dot spread estimates. The dot spread estimates are generally very close to the measured values.

The ΔE^*_{ab} vs. tone value for the dot spread estimates are shown in Figure 27. Cyan and magenta are significantly improved, with most of the errors less than 1.5 ΔE^*_{ab}, and a maximum error of approximately 2.5 ΔE^*_{ab} at 70%. Yellow improved slightly overall, though the maximum is now shifted to 60%, with a value of 3.0 ΔE^*_{ab}.

For the magenta 50% tone patch that was shown in Figure 2, the optimum value of the dot area increase was found to be $g = 0.21$. Figure 28 shows that the estimated and measured reflectance curves now agree much better, and the ΔE^*_{ab} is reduced to 1.64.

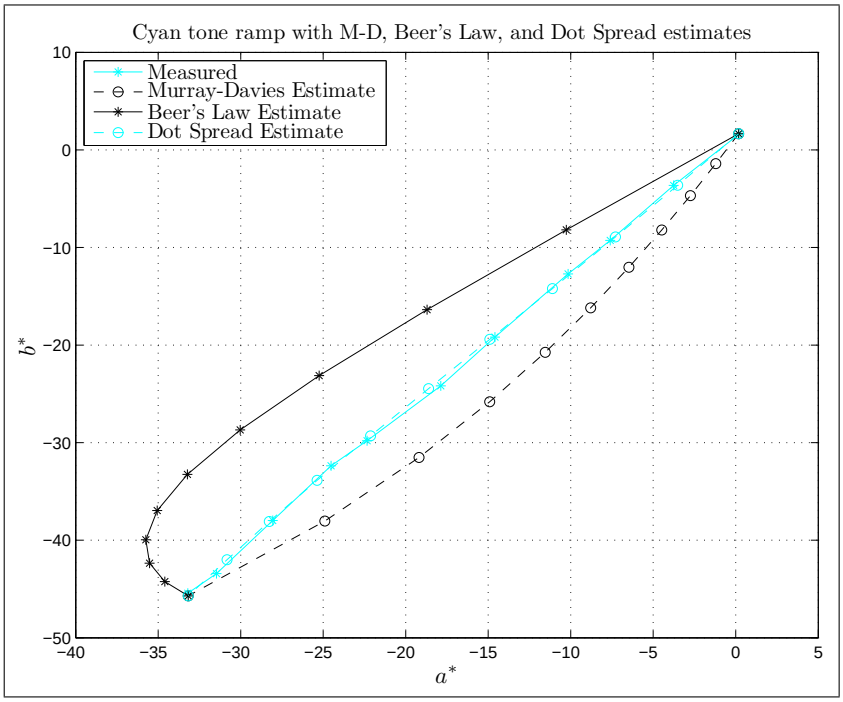

Figure 24: Cyan tone ramp, web offset, conventional screen, with Murray-Davies, Beer's Law, and Dot Spread estimates, coated matte paper.

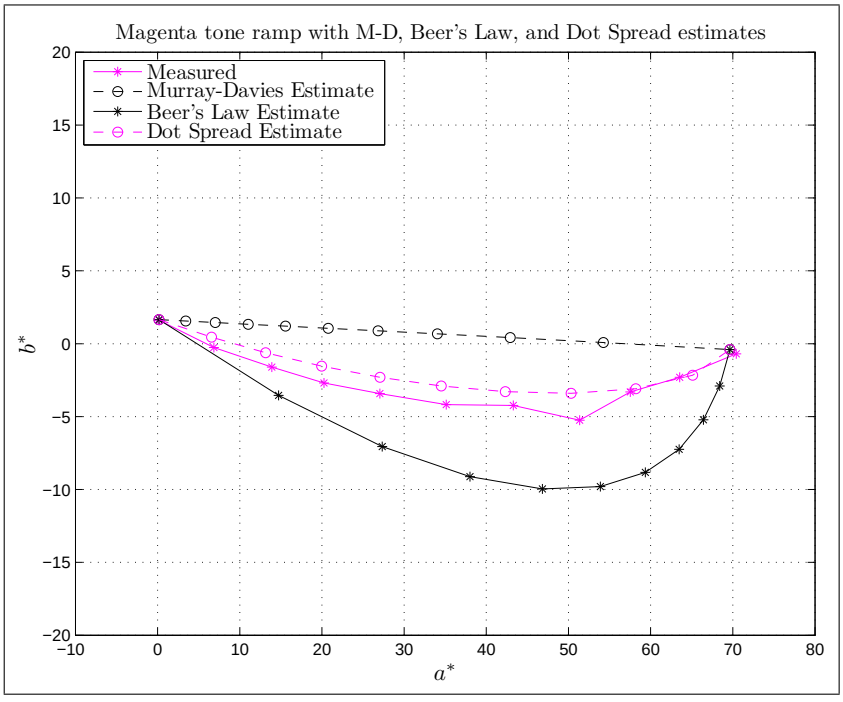

Figure 25: Magenta tone ramp, web offset, conventional screen, with Murray-Davies, Beer's Law, and Dot Spread estimates, coated matte paper.

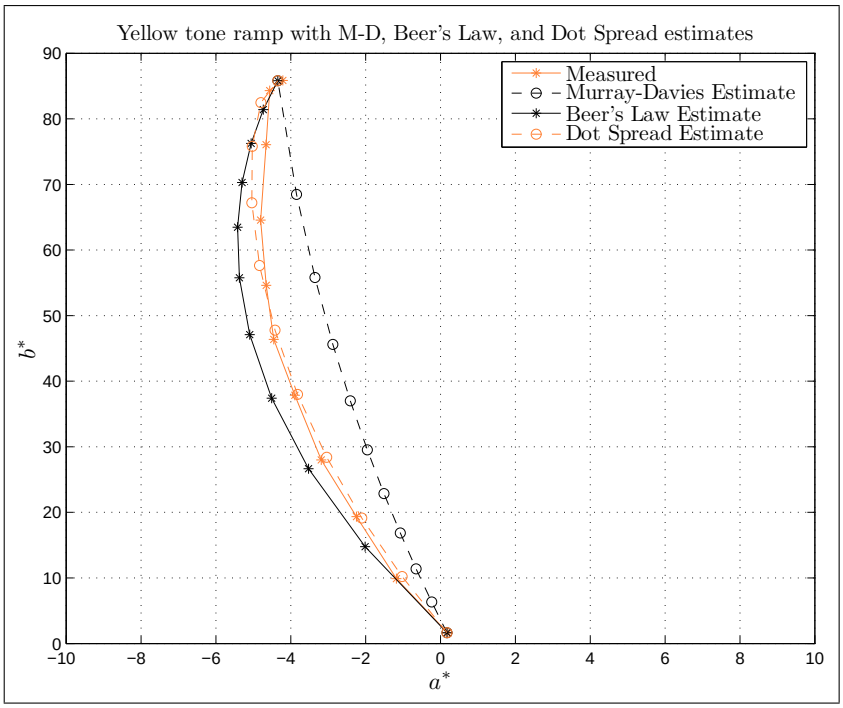

Figure 26: Yellow tone ramp, web offset, conventional screen, with Murray-Davies, Beer's Law, and Dot Spread estimates, coated matte paper.

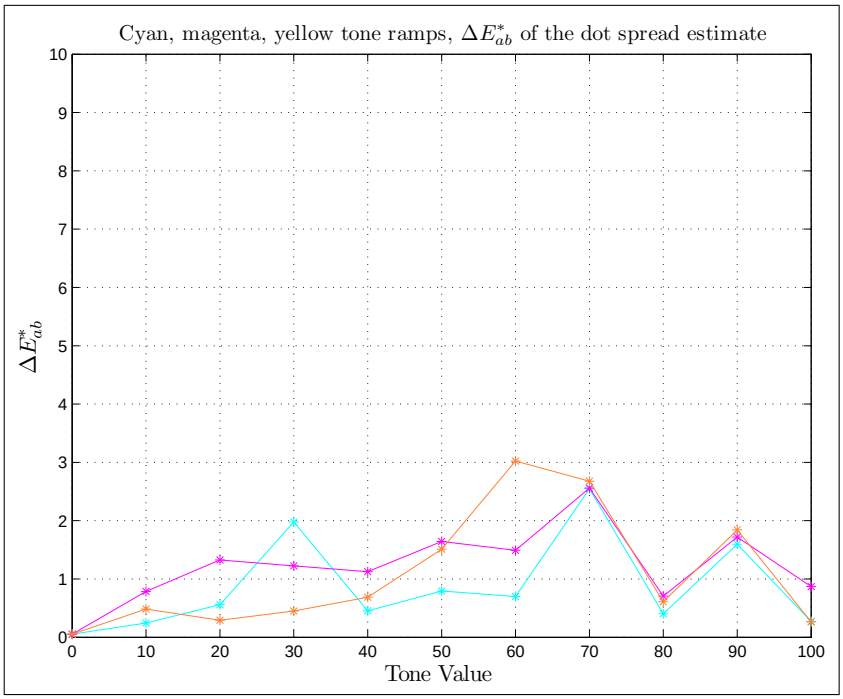

Figure 27: Cyan, magenta, yellow tone ramps, ΔE^*_{ab} values of the dot spread estimate, coated matte data.

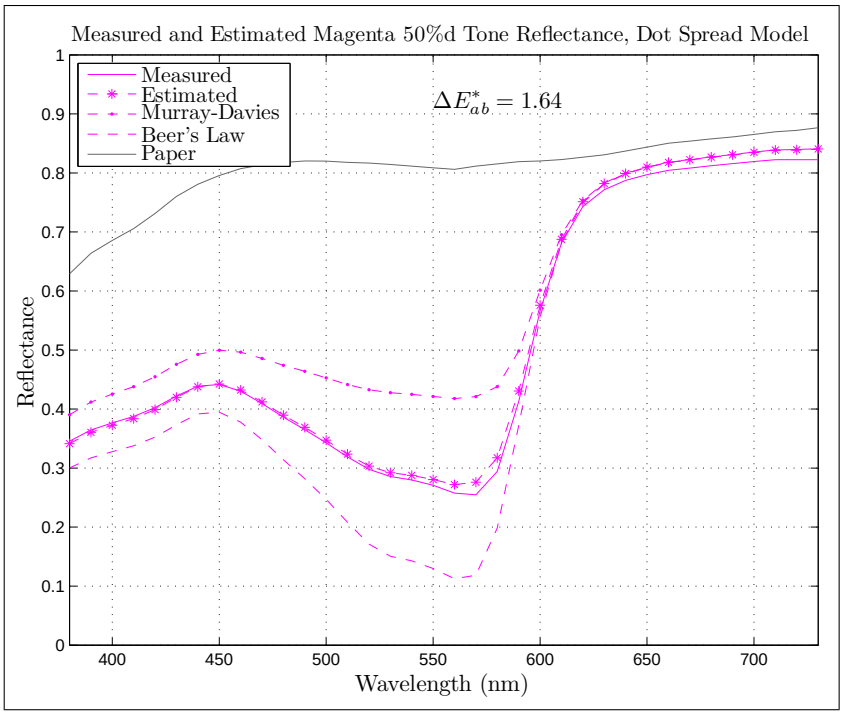

Figure 28: Magenta 50% tone reflectance, dot spread model, $g = 0.21$. The estimated reflectance now agrees much better with the measured reflectance.

Yule-Nielsen Model

Dot gain has historically been divided into two types: physical dot gain and optical dot gain (Wyble & Berns, 2000). The first dot gain is the enlargement of the dot as it goes through the printing process. This type of dot gain is best measured with a halftone dot planimeter, which utilizes a high resolution image of a halftone area to count the number of pixels encompassed in the halftone dots. For hard dots, such a planimeter can give good results. For softer dots, the determination of which pixels are part of the dot and which are not becomes problematic.

Various attempts have been made to model this physical dot gain, for example the GRL model (Viggiano, 1983). This particular model serves to create an estimate of the physical size of the dot on the paper to be used as input to an equation that estimates reflectance. Dr. Bjorn Kruse and his students have contributed to the literature of physical dot gain by suggesting models that allow one to estimate the physical spread of dots from an image of the idealized dot (Kruse & Wedlin (1995), Gustavson & Kruse (1996), and Kruse & Gustavson (1996)).

Unlike the dot spread model, there is a tacit assumption in the physical dot gain model that, although the dot is larger, it does not get thinner.

The second form of dot gain is called optical dot gain. Optical dot gain is caused when light enters the paper through a halftone dot, and emerges through the paper between dots. In this way, the paper between the dots is tinted by the color of the dots. As a result, the halftone area takes on a richer color than normally expected, based on the physical size of the dot and the Murray-Davies equation.

An equation was introduced at TAGA (Yule & Nielsen, 1951) which has been widely used among researchers as the basis of an equation modeling dot gain (for example, see Pearson (1980), Viggiano (1985), Pope (1989), Rolleston & Balasubramanian (1993), Arney et al. (1996), Hersch & Crt (2005), Gooran et al. (2009), Rossier & Hersch (2010)).

The Yule-Niesen equation is given by

$$R_{ht}^{(1/n)} = (1-a)R_p^{(1/n)} + aR_s^{(1/n)} \tag{9}$$

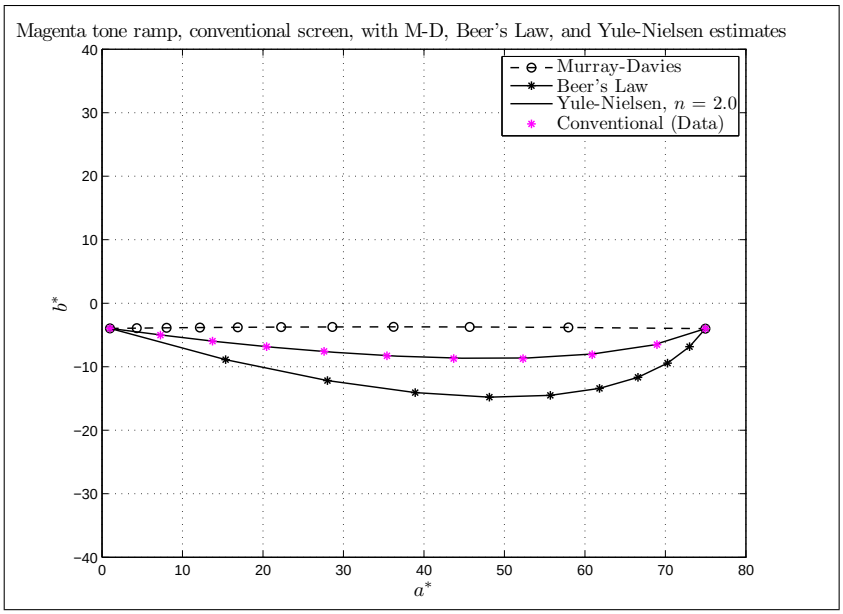

Figure 29: Magenta tone ramp, Rodriguez data, conventional screen. The Yule-Nielsen model with $n = 2.0$ closely matches the measured data.

or

$$R_{ht} = \left((1-a) R_p^{(1/n)} + a R_s^{(1/n)} \right)^n \tag{10}$$

Yule-Nielsen was *originally intended* to explain the optical dot gain. According to Ruckdeschel & Hauser (1978), the value for n should lie between 1 and 2. Pearson (1980) narrowed this range down to between 1.4 and 1.8 with a recommended value of 1.7. However, various researchers have found it necessary to go beyond this range.

Pope (1989) calculated n-values for 35 patches on the same substrate. He found unusual results when computations were based on the "off channels". For example, the n-value for cyan as measured through the blue channel was as small as 0.10, which shows dot shrinkage. Infinite n-values were seen in cyan as computed from the green channel.

Viggiano (2010) used a negative n, with the following justification:

> *Lewandowski, et al., have reported negative values of n when fitting the VHM-1 to spectra of halftones printed on ceramics, and the current author has provided the theoretical explanation of spreading of scattering ink. In this paper, the penetration of ink into the substrate is offered as an additional cause for this phenomenon. Both theoretical and empirical justification are offered to support this contention.*
>
> *The theoretical justification is based on the remarkable similarity between the Yule-Nielsen formula with $n = -1$ and the ratio K/S used in colorant formulation work. Empirical data were generated by printing rather coarse halftone patterns on fiber inkjet paper, using ink jet with dye-based inks. The fitted value of n was approximately -3.8, versus fitted n values ranging from approximately +3.8 to +5.8 for prints produced on media that do not permit penetration.*

Figure 29 shows that the Yule-Nielsen formula, with $n = 2.0$, does a very good job of fitting the Rodriguez data, magenta with conventional screening. Figure 30 shows that $n = 4.5$ is a very good fit to the magenta stochastic data. The fact that the Yule-Nielsen curve at $n = 4.5$ comes very close to the Beer's Law estimate is no accident. The Yule-Nielsen equation converges to the Beer's Law equation as $n \to \infty$. According to Viggiano (2010), this fact was recognized by Pollack (1955).

Figure 31 shows the Yule-Nielsen estimates for magenta halftones with dot areas of 20%, 40%, 60%, and 80%. The bowed lines are for n-values of 1 (Murray-Davies), 1.2, 1.5, 2.0, 3.0, 6.0, and ∞ (Beer's Law). As can be seen, the dot areas and n-values form a grid that covers the area such that any particular (a^*, b^*) value has a unique dot area and n-value associated with it.

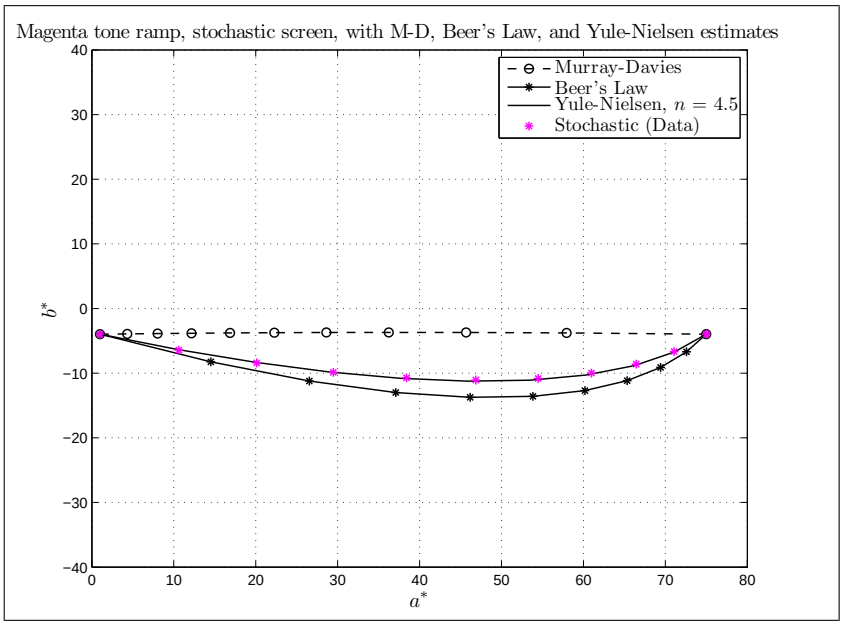

Figure 30: Magenta tone ramp, Rodriguez data, stochastic screen. The Yule-Nielsen model with $n = 4.5$ closely matches the measured data.

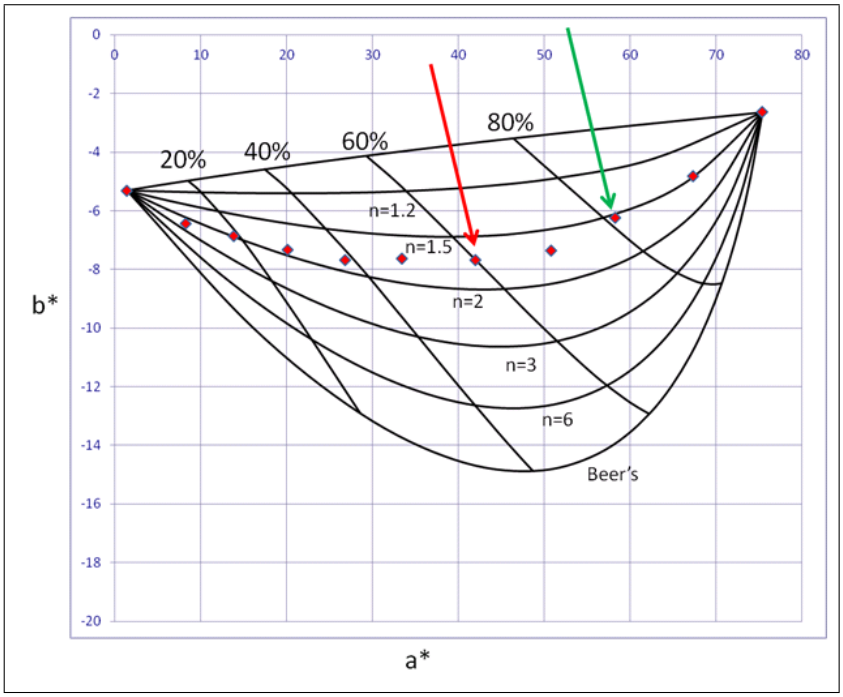

Figure 31: Yule-Nielsen estimates for magenta halftones, with n-values of 1 (Murray-Davies), 1.2, 1.5, 2.0, 3.0, 6.0, and ∞ (Beer's Law).

The red diamonds are measurements of an actual magenta tone ramp. The red diamond marked with the red arrow is a 60% halftone. Its coordinates in terms of the Yule-Nielsen parameters are $a = 60\%$, $n = 1.7$. The red diamond marked with a green arrow is an 80% halftone. The Yule-Nielsen parameters are $a = 81\%$, and $n = 1.53$.

The color of a 60% halftone can slide up and down along the 60% Yule-Nielsen line, but there does not seem to be much right-to-left translation. From this data set, it would appear there is no need for the dot area in the Yule-Nielsen equation to be a free parameter.

It would appear, however, that the n-value is a function of the tone value. At the 10% and 20% tone values, the n-value is 2.0 or larger. It gradually decreases with tone value, down to an n-value of 1.5 at 90% tone value.

There is a subtle but very important point to be made here – a shift in thinking. We are used to thinking about the Yule-Nielsen n-value as being a constant for any given printing condition, independent of tone value. We also think of the TVI as very much a function of tone value. Figure 31 suggests that the appropriate way to look at the color of a halftone is that the tone value that is used in the Yule-Nielsen equation is equal to the initial tone value (i.e. the area on the plate). In other words, the TVI is always zero.

The n-value is the parameter which changes as a function of tone value, and also the parameter which changes with the print conditions. The n-value has taken the place of TVI as the parameter that defines the print conditions and which must be monitored on press.

Murray-Davies-Beer Linear Equation

The Yule-Nielsen equation and the dot spread equation give very similar results when viewed in color space. It would be hard to select one over the other in terms of how well the two models fit actual data.

Either equation could be used to define a parameter that could be used as a process control parameter in place of TVI. One would compute a Yule-Nielsen n-value curve or a dot area increase curve instead of the standard TVI curve. The benefit to using one of these equations over the standard Murray-Davies equation is that either of the newer equations would provide a more accurate estimate of the CIELAB value of the halftone.

Unfortunately, while it is a rather simple calculation to determine the Murray-Davies TVI, both the Yule-Nielsen equation and the dot spread equation are considerably more complicated equations, and neither one can be solved in closed form. Given a set of measurements (paper, solid, and halftone), an iterative procedure must be used to determine the Yule-Nielsen n-value or the dot area increase value, g. While either equation would be a beneficial replacement for the Murray-Davies TVI equation, the calculation difficulty limits the utility. Thus, there is a need for an equation which provides more accurate colorimetric estimates than Murray-Davies, but which is easier to solve than the Yule-Nielsen or dot spread equations.

The fact that the "rungs of the ladder" in Figure 31 are very close to linear suggests one much simpler equation. It is assumed that the color of a halftone patch will lie at some point that is close to a straight line between the Murray-Davies estimate of the color of that halftone and the Beer's Law estimate of the color of that halftone. In other words,

$$\widehat{(L^*,a^*,b^*)}_{ht} = h \cdot \widehat{(L^*,a^*,b^*)}_{ht,MD} + (1-h) \cdot \widehat{(L^*,a^*,b^*)}_{ht,BL} \tag{11}$$

In reflectance space,

$$\hat{R}_{ht} = h \cdot \hat{R}_{ht,MD} + (1-h) \cdot \hat{R}_{ht,BL} \tag{12}$$

In Equations 11 and 12, h is the dot hardness parameter which adjusts the balance between hard dots ($h = 1$) and continuous tone ($h = 0$). The subscripts "MD" and "BL" denote the Murray-Davies and Beer's Law models of the halftone color or reflectance, respectively, and the hat ($\hat{}$) symbols are used to denote estimates.

To determine the optimum value of h for a particular halftone, one needs the spectrum of the paper, the spectrum of the solid, and the tone value (i.e. dot area on the plate). Equation 1 is used to compute the Murray-Davies estimate of the spectrum at that tone value, and from this spectrum, the value for $\widehat{(L^*,a^*,b^*)}_{ht,MD}$. Similarly, Equation 4 is used to compute the Beer's Law estimate of the spectrum and from that the Beer's Law estimate of the CIELAB value of the halftone, $\widehat{(L^*,a^*,b^*)}_{ht,BL}$.

The optimum value of h is that value which minimizes the ΔE^*_{ab} between the measured CIELAB value of the halftone, $(L^*,a^*,b^*)_{ht}$

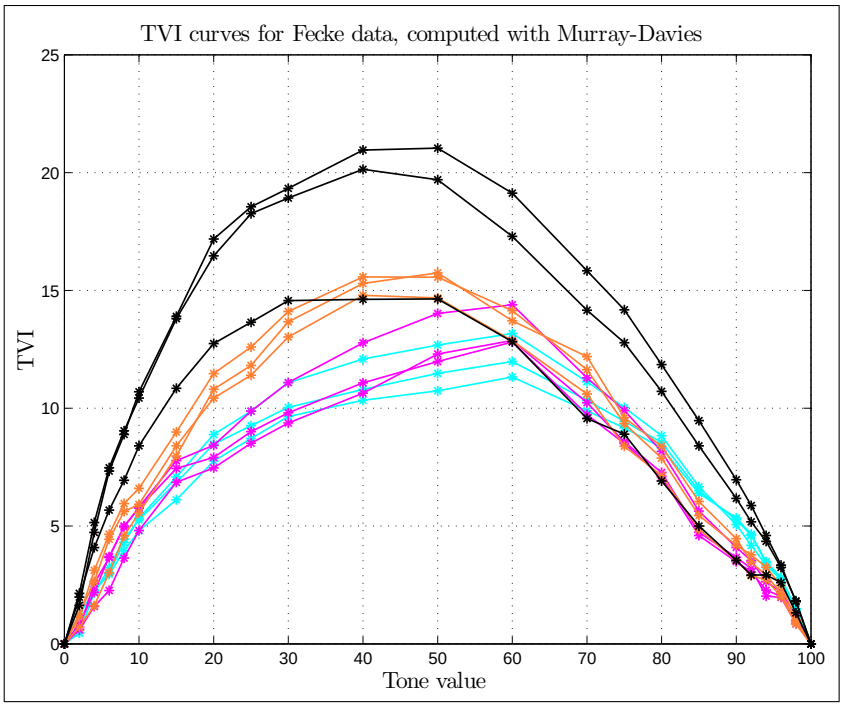

Figure 32: TVI curves for Fecke data.

and the estimated CIELAB value, $\widehat{(L^*,a^*,b^*)}_{ht}$. Alternately, one may compute the value of h that minimizes the difference between the measured reflectance and the estimated reflectance as computed in Equation 12.

The least squares solution for h in (L^*,a^*,b^*) space is relatively simple. Dropping the subscript ht (since we're using only terms for a halftone), we have

$$h = \frac{(L^* - \widehat{L^*}_{MD})(\widehat{L^*}_{BL} - \widehat{L^*}_{MD}) + (a^* - \widehat{a^*}_{MD})(\widehat{a^*}_{BL} - \widehat{a^*}_{MD}) + (b^* - \widehat{b^*}_{MD})(\widehat{b^*}_{BL} - \widehat{b^*}_{MD})}{(\widehat{L^*}_{BL} - \widehat{L^*}_{MD})^2 + (\widehat{a^*}_{BL} - \widehat{a^*}_{MD})^2 + (\widehat{b^*}_{BL} - \widehat{b^*}_{MD})^2} \tag{13}$$

The least squares solution for h in reflectance space follows the same form as Equation 13, but instead of three terms in the numerator and denominator for each of the (L^*,a^*,b^*) color components, we have similarly formed terms for each wavelength interval, λ_i, as shown in Equation 14. This may be easily computed in spreadsheets or other data analysis software.

$$h = \frac{\sum_{\lambda_i} \left(R(\lambda_i) - \hat{R}_{MD}(\lambda_i)\right) \cdot \left(\hat{R}_{BL}(\lambda_i) - \hat{R}_{MD}(\lambda_i)\right)}{\sum_{\lambda_i} \left(\hat{R}_{BL}(\lambda_i) - \hat{R}_{MD}(\lambda_i)\right)^2} \tag{14}$$

Test of the MDB Linear Equation, Fecke Data

The data for this test is from Paul Fecke, formerly of QuadGraphics. Three test targets were measured – one with water nominal, one with water high, and one with water low. The data used includes tone ramps for cyan, magenta, yellow, and black.

In the first part of this experiment, the TVI was computed using the conventional Murray-Davies method (Equation 3). In Figure 32, we see the computed TVI vs. tone value. The effective dot area (computed with Equation 2), the spectrum of the paper, and the spectrum of the solid were then used to estimate the spectra and CIELAB values at each of the tone values available. The estimated and measured CIELAB values were then compared, and the resulting ΔE^*_{ab} color differences are shown in Figure 33.

The dot hardness value was then computed using Equation 13, and the optimum dot hardness value vs. tone value is shown in Figure 34. As before, the spectrum of the paper and the spectrum of the solid were used along with the optimum dot hardness

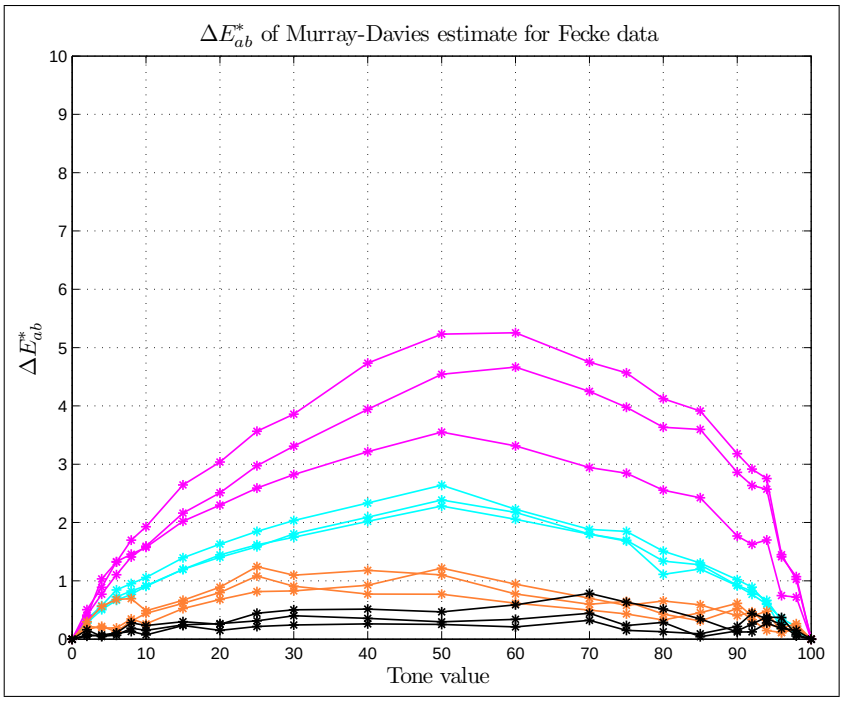

Figure 33: ΔE^*_{ab} values of the Murray-Davies estimate, Fecke data.

values to estimate the spectra and CIELAB values at each of the tone values available. The estimated and measured CIELAB were then compared, and the resulting ΔE^*_{ab} color differences are shown in Figure 35.

As can be seen from Figure 35, the errors in the color estimates are nearly all below 1 ΔE^*_{ab}. The worst of all the errors in the Murray-Davies method – the errors in the magenta midtones – have been reduced from the range of 3.5 to 5.2 ΔE^*_{ab} to under 1 ΔE^*_{ab}. The estimation errors for black have surprisingly increased, but they were quite small to begin with.

Test of the MDB Linear Equation, Bestman Data

The data for this test is from Dr. Bestman, which consists of CMYK tone ramps for conventional and stochastic screens. As with the Fecke data, we computed the TVI with the Murray-Davies method, the optimum dot hardness values, and the corresponding CIELAB and ΔE^*_{ab} values. The results are shown in Figures 36 through 39. For the Murray-Davies method, the ΔE^*_{ab} values are just over 8 for magenta stochastic, and with the dot hardness method, the ΔE^*_{ab} values are again almost all less than 1.

Test of the MDB Linear Equation, Hallam Gravure Data

The data for this test is from Bob Hallam, which consists of CMY tone ramps for gravure data. Once again, we compute the TVI, the optimum dot hardness values, and the corresponding CIELAB and ΔE^*_{ab} values. The results are shown in Figures 40 through 43. The Murray-Davies method yields ΔE^*_{ab} values around 9 for magenta midtones, and the dot hardness method yields ΔE^*_{ab} values substantially less than 1 for yellow, and less than 3.5 for cyan and magenta.

Dot Hardness Dependence on Tone Value

As can be seen from the Bestman data in Figure 38, the dot hardness values tend to decrease with increasing tone value. This is also apparent in the Fecke data (Figure 34), though to a lesser degree. The Hallam gravure data also follows this trend (Figure 42), apart from an unexplained anomaly with magenta below 30% tone value. It is also interesting to note how the conventional screen dots have a higher hardness value than for stochastic. The dependence on tone value (or screen type) is likely because, as dots get bigger (or closer together for stochastic), they are more likely to touch, so ink is more likely to flow on the paper, approximating more of a continuous tone model. This is in agreement with the fact that the dot area increase curves tended to lean toward

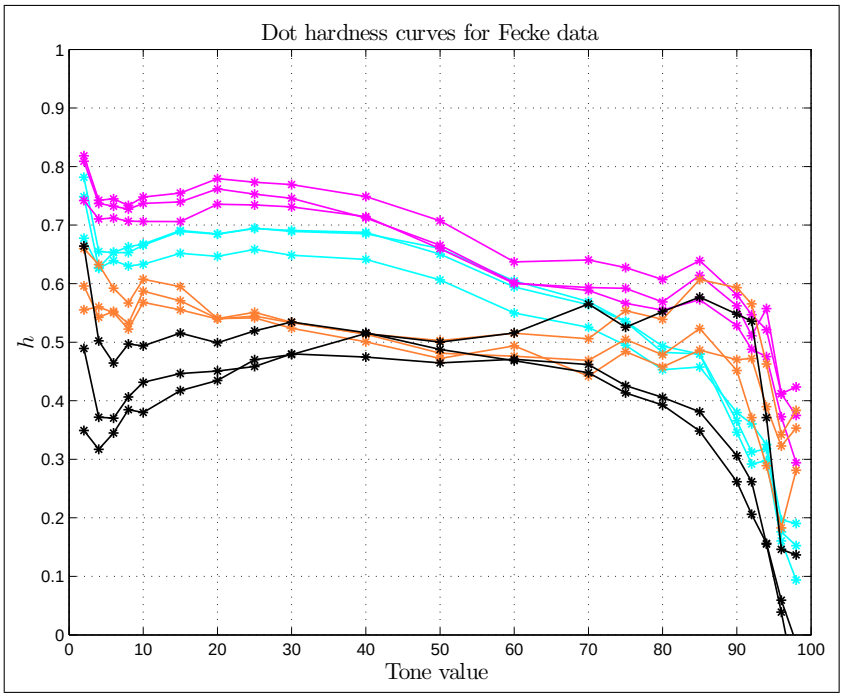

Figure 34: Dot hardness vs. tone value, Fecke data.

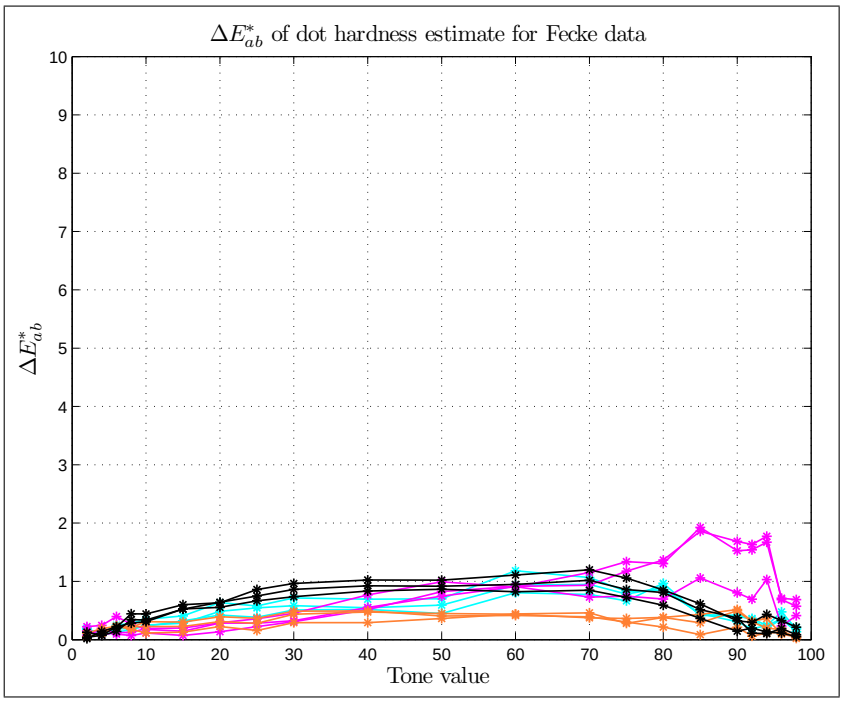

Figure 35: ΔE^*_{ab} values of the MDB linear (dot hardness) estimate, Fecke data.

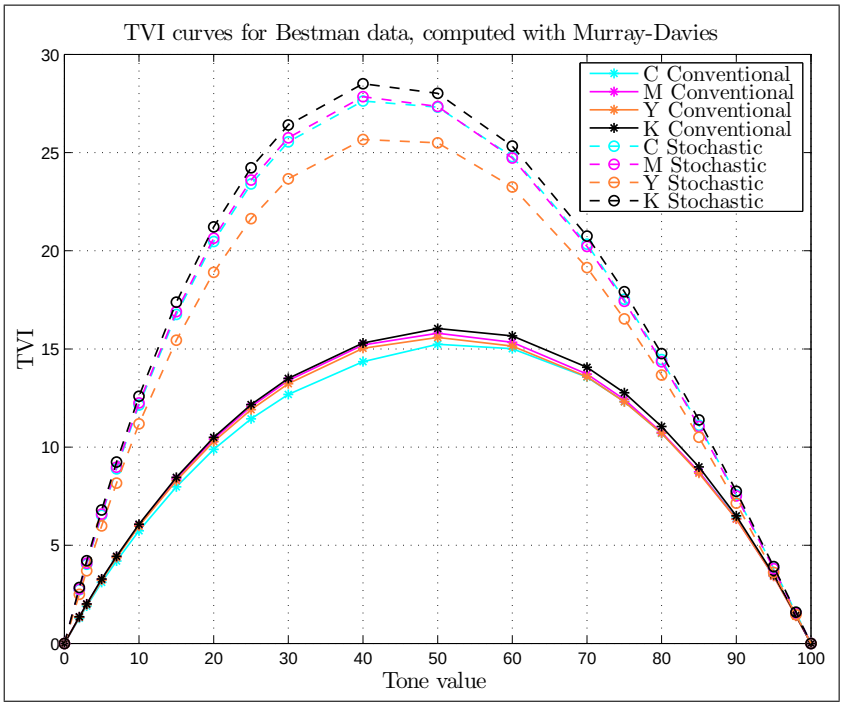

Figure 36: TVI curves for Bestman data, conventional and stochastic line screens.

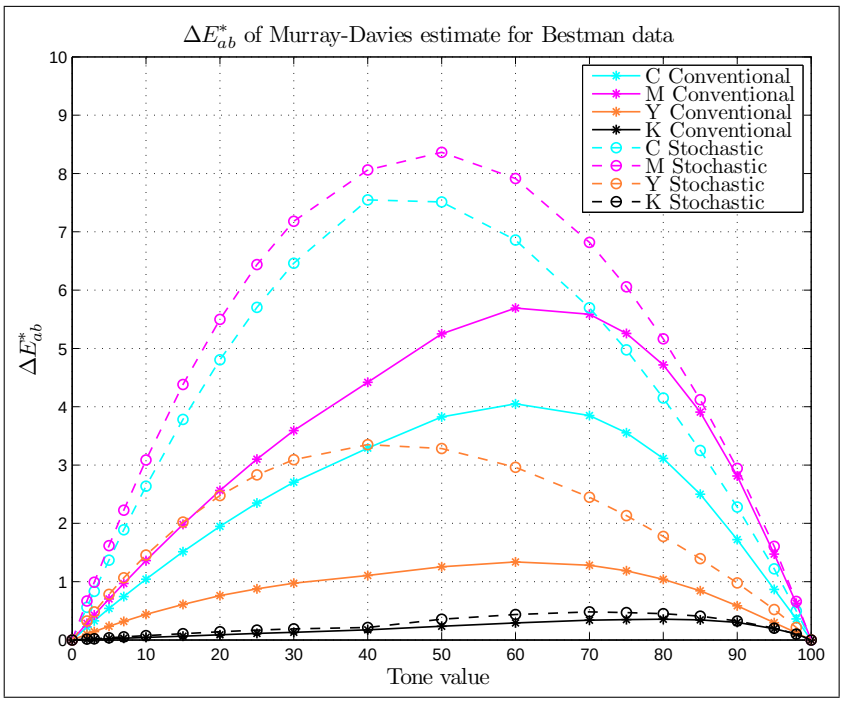

Figure 37: ΔE^*_{ab} values of the Murray-Davies estimate, Bestman data.

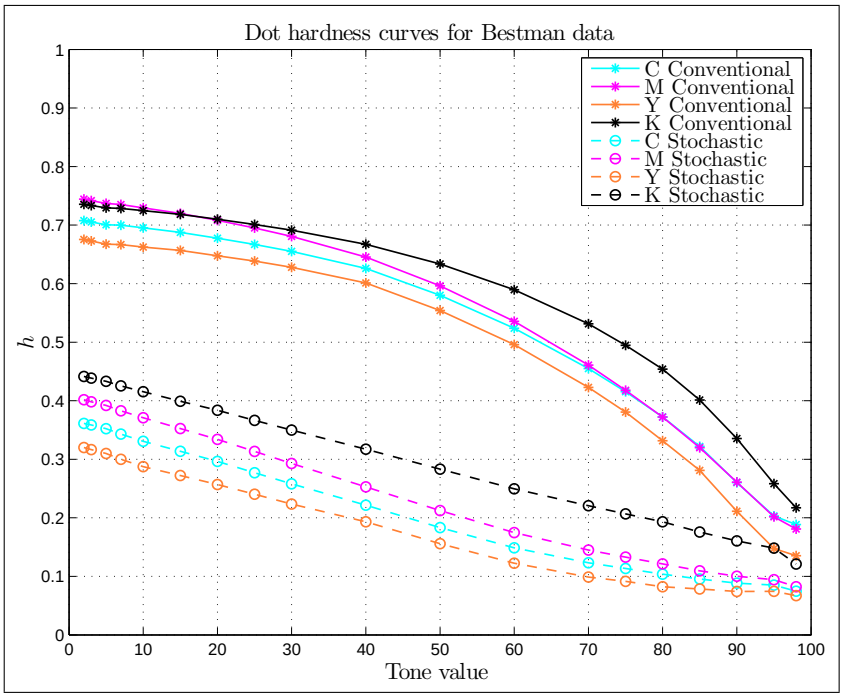

Figure 38: Dot hardness vs. tone value, Bestman data.

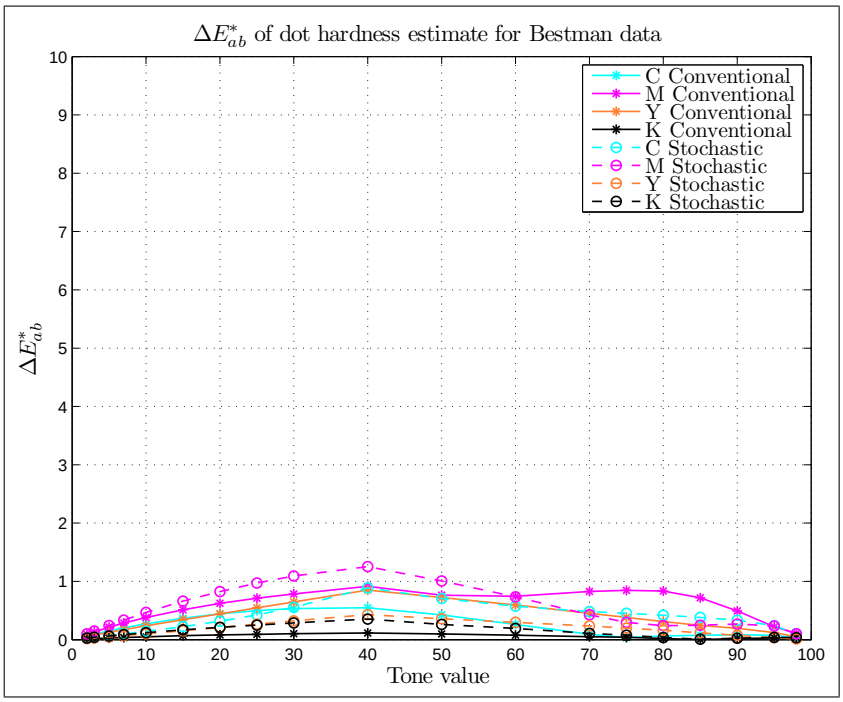

Figure 39: ΔE^*_{ab} values of the MDB linear (dot hardness) estimate, Bestman data.

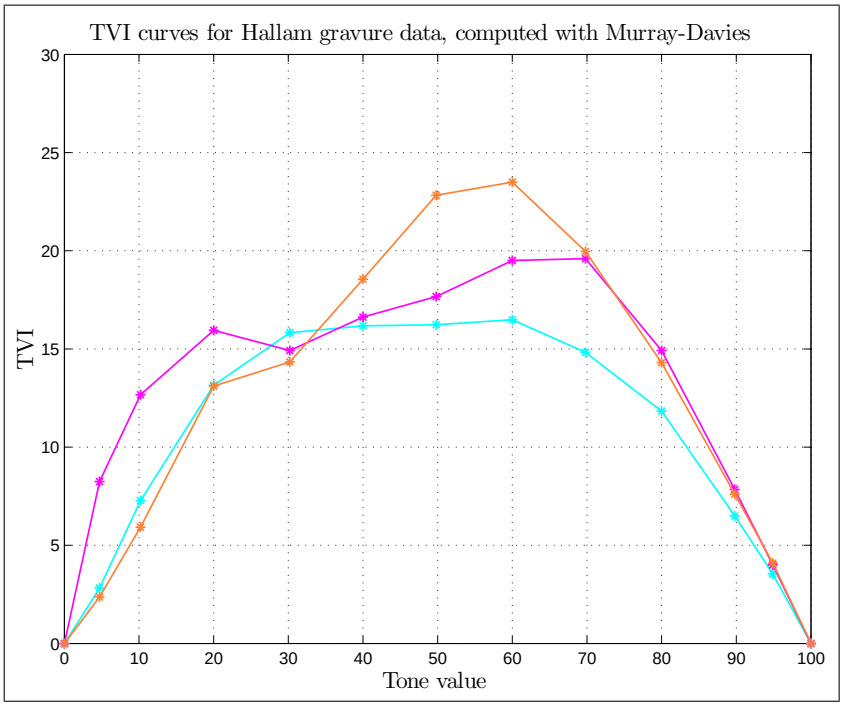

Figure 40: TVI curves for Hallam gravure data.

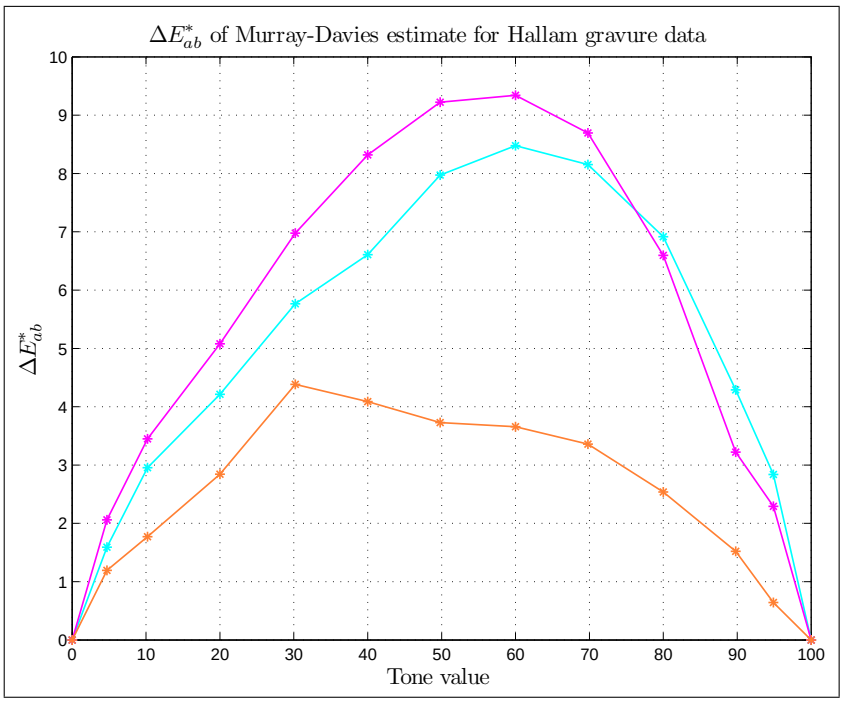

Figure 41: ΔE^*_{ab} values of the Murray-Davies estimate, Hallam gravure data.

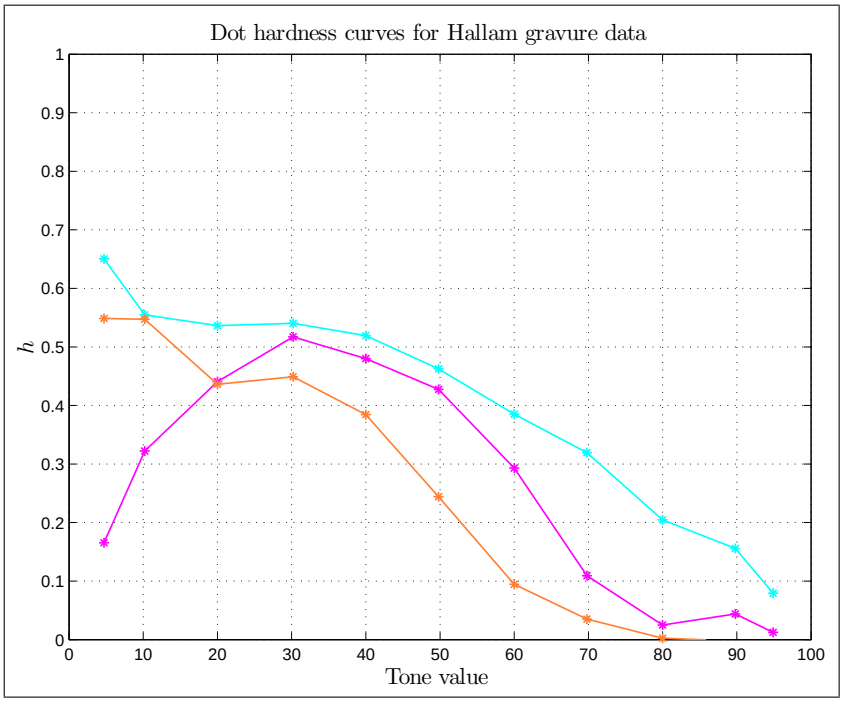

Figure 42: Dot hardness vs. tone value, Hallam gravure data.

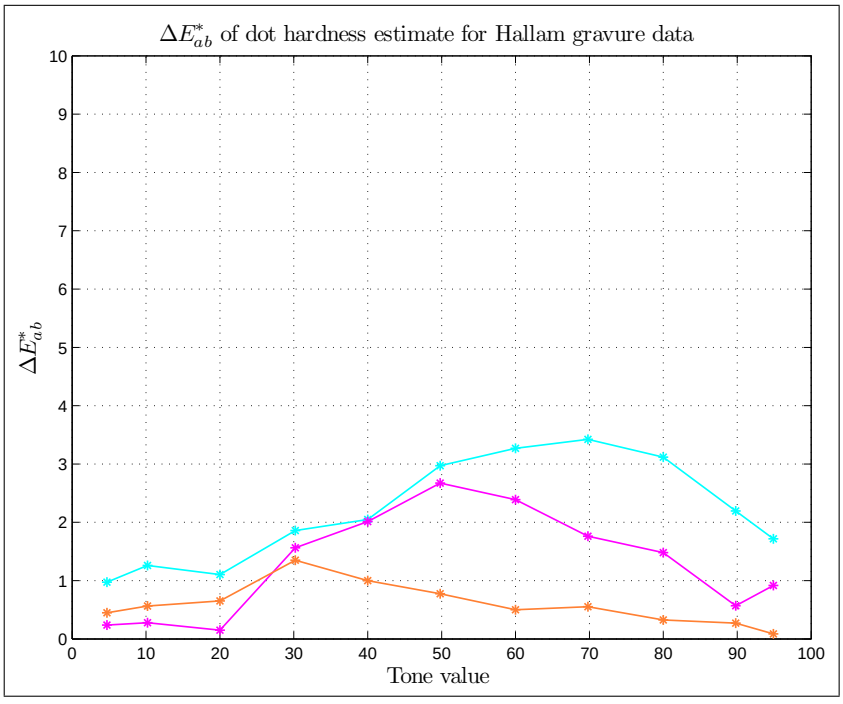

Figure 43: ΔE^*_{ab} values of the MDB linear (dot hardness) estimate, Hallam gravure data.

smaller tone values.

The dependence on tone value is one potential limitation in the utility of the Murray-Davies-Beer linear equation – one must determine a dot hardness curve parametrically (perhaps with a linear model with negative slope as a first-order approximation), or independently at each tone value. If dot hardness value is to be used as a process control parameter, one must first understand the shape of the dot hardness curve for the printing conditions of interest.

Then again, one might question how much dot hardness or dot spread (or Yule-Nielsen n-value) can be "process controlled." The Bestman data suggests there is a strong correlation between dot hardness and the screen type. The Hallam gravure data (having smaller values of h than for conventional screens) suggests the viscosity of the ink may be a crucial factor. Though it was not shown in the graphs of the Fecke data, there was surprisingly not a strong correlation between water levels and dot hardness. The type of paper (especially coated vs. uncoated) is also likely to impact how much a dot can spread. These issues will be studied in future work.

Conclusions

The established way of talking about TVI is based on the Murray-Davies equation, which assumes hard dots. This paper demonstrates that the Murray-Davies equation is a poor estimator of spectra (and hence color), especially for cyan and magenta halftones. This held for all types of printing that were investigated.

Beer's law is an alternative model which is based on continuous tone printing. This equation is found to be a good estimator for gravure and stochastic web offset, but does not work quite as well for conventional halftoned web offset.

These two equations (Murray-Davies and Beer's law) are shown to provide boundaries between which all halftone printing seems to fall. That is to say, any printing condition can be described as fitting somewhere along a continuum from hard dots to soft dots to continuous tone. The position along the continuum, effectively the dot hardness parameter, can serve as a replacement for TVI to accurately predict spectra and CIELAB values, and is universal across all printing types. It may also be useful as a process control parameter.

Three different equations were used to characterize the position along this continuum: the dot spread equation, Yule-Nielsen, and Murray-Davies-Beer linear. The three are very similar in results, but the MDB linear equation can be directly solved for the dot hardness parameter.

Appendix A

This paper relies heavily on Beer's Law to estimate spectra. However, spectral data is not always available. Clearly it would be advantageous if the Beer's Law estimate could be derived from (L^*, a^*, b^*) values. To test this, the Beer's Law estimate was computed using two different methods for one particular cyan sample.

The first method was the standard method, where the Beer's Law calculation is done at every wavelength based on the spectra of the paper and the solid.

For the second method, the (L^*, a^*, b^*) values for the paper and solid cyan were converted to XYZ values. Since there is a fairly large width of the tristimulus filters, the XYZ values were converted to LMS values via the Bradford transform. This will reduce the width of the filters as much as possible.

The LMS values were then used in the Beer's Law equation to get estimated LMS values. These estimates were then converted to XYZ values and then to (L^*, a^*, b^*) values.

The results on just this one ink were poor, as shown in Figure 44. The maximum color difference between the two methods was quite close to 4 ΔE^*_{ab}. The other inks were not tested.

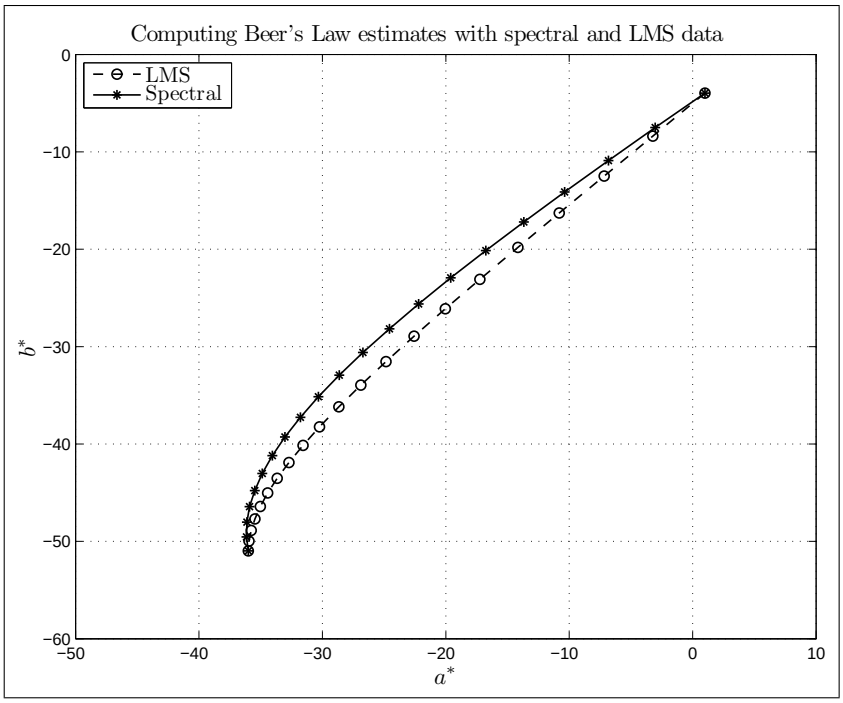

Figure 44: Using Beer's Law with spectral data and in LMS color space. For this particular sample, the maximum color difference between the two methods was approximately 4 ΔE^*_{ab}.

Appendix B

The curves used for TVI and dot area increase are linear combinations of three basis functions. For an input area, a, where $0 \leq a \leq 1$, the three basis functions are given by

$$p_1(a) = -4 \cdot a \cdot (a-1) \tag{15}$$

$$p_2(a) = 21 \cdot a \cdot (a-1) \cdot (a-0.5) \tag{16}$$

$$p_3(a) = -64 \cdot a \cdot (a-1) \cdot (a-0.5)^2 \tag{17}$$

The magnitude of each of these basis functions are referred to as the *gain*, *lean*, and *bulge* parameters. The parametric curve is therefore given by

$$curve(a) = gain \cdot p_1(a) + lean \cdot p_2(a) + bulge \cdot p_3(a) \tag{18}$$

Literature Cited

Arney, J. S., Arney, C. D., & Engeldrum, P. G. (1996). Modeling the yule-nielsen halftone effect. *Journal of Imaging Science and Technology*, *40*(3), 233–238.

Bestman, G. (2011). Action items from Berlin meeting, document N1162. Presented at ISO TC 130 meeting in Sept. 2011.

Gooran, S., Namedanian, M., & Hedman, H. (2009). A new approach to calculate colour values of halftone prints. In *IARAGAI*.

Gustavson, S., & Kruse, B. (1996). Evaluation of a light diffusion model for dot gain. In *TAGA Proceedings*, (pp. 58–69).

Hersch, R. D., & Crt, F. (2005). Improving the Yule-Nielsen modified spectral Neugebauer model by dot surface coverages depending on the ink superposition conditions. In *IS&T Electronic Imaging Symposium, Conf. Imaging X: Processing, Hardcopy and Applications, SPIE*, vol. 5667, (pp. 434–445).

ISO 10128 (2009). Graphic technology – methods of adjustment of the colour reproduction of a printing system to match a set of characterisation data.

Kruse, B., & Gustavson, S. (1996). Dot gain modeling applied to stochastic screens. In *TAGA Proceedings*, (pp. 50–57).

Kruse, B., & Wedlin, M. (1995). A new approach to dot gain modeling. In *TAGA Proceedings*, (pp. 329–338).

Pearson, M. (1980). N-value for general conditions. In *TAGA Proceedings*, (pp. 415–425).

Pollack, F. (1955). The relationship between the densities and dot sizes of multi-colour halftone images. *Journal of Photographic Science*, *3*(4), 308–313.

Pope, W. (1989). A practical approach to N-value. In *TAGA Proceedings*, (pp. 142–151).

Rolleston, R., & Balasubramanian, R. (1993). Accuracy of various types of Neugebauer model. In *IS&T and SID's Color Imaging Conference: Transforms and Transportability of Color*, (pp. 32–37).

Rossier, R., & Hersch, R. D. (2010). Ink-dependent n-factors for the Yule-Nielsen modified spectral Neugebauer model. In *CGIV – Fifth European Conference on Colour in Graphics, Imaging, and MCS/10 Vision 12th International Symposium on Multispectral Colour Science*.

Ruckdeschel, F. R., & Hauser, O. G. (1978). Yule-Nielsen effect in printing: A physical analysis. *Applied Optics*, *17*(21), 3376–3383.

Seymour, J. (2007). How many ΔEs are there in a ΔD? In *TAGA Proceedings*, (pp. 311–348).

Seymour, J. (2008). Building a bridge from Dense City to Colorimetropolis. In *TAGA Proceedings*, (pp. 202–231).

Viggiano, J. A. S. (1983). The GRL dot gain model. In *TAGA Proceedings*, (pp. 423–440).

Viggiano, J. A. S. (1985). The color of halftone tints. In *TAGA Proceedings*, (pp. 647–663).

Viggiano, J. A. S. (2010). Ink penetration, isomorphic colorant mixing, and negative values of Yule-Nielsen n. In *18th Color Imaging Conference Final Program and Proceedings*.

Wyble, D. R., & Berns, R. S. (2000). A critical review of spectral models applied to binary color printing. *Color Research and Application*, *25*, 4–19.

Yule, J. A. C., & Nielsen, W. J. (1951). The penetration of light into paper and its effect on halftone reproduction. In *TAGA Proceedings*, (pp. 65–76).